Nuclear Magnetism in Copper, Silver, and Rhodium Metals at Positive and Negative Spin Temperatures in the Nano- and Picokelvin Regimes

Olli V. Lounasmaa

Hahn–Meitner Institut, 14019 Berlin, Germany

and

Low Temperature Laboratory, Helsinki University of Technology, 02150 Espoo, Finland

Abstract

This paper reviews magnetic susceptibility and neutron diffraction studies of metallic copper, silver, and rhodium. I shall start by giving a short historical introduction, followed by a simple theoretical discussion. The concept of negative spin temperatures will then be explained. Next, I shall describe the experimental techniques. The results of measurements will then be presented, first on copper, then on silver, and lastly on rhodium. My review ends with a few concluding remarks.

1 Introduction

Electronic magnetism shows a wide spectrum of different ordering phenomena, extending from room temperature and above in iron to a few millikelvins in cerium magnesium nitrate. Because the nuclear magnetic moments are three orders of magnitude smaller than their electronic counterparts and because dipolar interactions are proportional to the respective magnetic moments squared, spontaneous ordering phenomena can be expected to occur in a nuclear spin system only at microkelvin temperatures and below. Solid ^{3}He is an exception owing to the strong quantum mechanical exchange force, augmented by the large zero-point motion, and so are Van Vleck paramagnets, like $PrNi_5$, in which considerable hyperfine enhancement of the magnetic field occurs. In these systems, the transition temperature is relatively high, around 1 mK (Andres and Bucher, 1968).

Experiments on nuclear magnetic ordering in metals are based on the pioneering investigations of Nicholas Kurti and his collaborators (Kurti et al., 1956). They established the feasibility of the "brute force" nuclear demagnetization method.

The basic formula for nuclear cooling is given by the relationship

$$B_1/T_1 = B_2/T_2\,, \tag{1}$$

where B_1 and T_1 are the initial and B_2 and T_2 the final magnetic field and temperature before and after demagnetization, respectively. In spite of the limitations imposed by cryogenic techniques forty years ago, the Oxford group succeeded in reaching 1 μK in the nuclear spin system of copper. Subsequent improvements in experimental procedures, much of it done in Helsinki after the advent of powerful dilution refrigerators and superconducting magnets in the late sixties, have made nuclear cooling a reality even below 1 nK (Lounasmaa, 1989).

It is important to note that very near the absolute zero it is meaningful to speak about two distinct temperatures in the same specimen and at the same time; these are the nuclear spin temperature T and the lattice and conduction electron temperature T_e. During nuclear refrigeration experiments, these two quantities can differ by many orders of magnitude. The nuclei reach local thermal equilibrium among themselves in a time characterized by τ_2, the spin–spin relaxation time, whereas the approach to equilibrium between nuclear spins and conduction electrons is governed by the spin–lattice relaxation time τ_1. At low temperatures, $\tau_2 \ll \tau_1$, which makes a separate nuclear spin temperature meaningful and real.

According to Korringa's law (Korringa, 1950),

$$\tau_1 T_e = \kappa\,, \tag{2}$$

where κ is Korringa's constant. For copper $\kappa = 1.2$ sK, in silver and rhodium $\kappa = 10$ sK, and in platinum $\kappa = 0.03$ sK. For example, at the conduction electron temperature of 50 μK, relevant to experiments on copper, the relaxation time $\tau_1 = 7$ h. In silver and rhodium the conduction electrons have been cooled to 100 μK; 28 h are then needed to reach equilibrium between electrons and nuclei in these metals. In low applied fields ($B < B_{\rm loc}$), the relaxation is faster at least by a factor of two and even quicker in the presence of electronic magnetic imputities. For example, in silver at 100 μK, $\tau_1 \approx 8$ h was actually observed after demagnetization. In platinum, conduction electrons and the nuclei are usually at the same temperature because of the very quick spin–lattice relaxation process.

Purcell and Pound (1951) first produced negative spin temperatures by rapid magnetic field reversal, using LiF as the working substance. The implications of these early NMR experiments have been discussed by Ramsey (1956) and by Van Vleck (1957). Two decades later, beginning in 1968, studies of nuclear co-operative phenomena at positive and negative spin temperatures were started by Abragam and Goldman (Abragam, 1987; Goldman, 1970; Bouffard et al., 1994); the Saclay group investigated the dielectric materials CaF_2, LiF, and LiH.

The Helsinki investigations of spontaneous nuclear magnetic ordering were started in the mid 1970's by constructing a two-stage nuclear demagnetization cryostat, a pioneer of its kind (Ehnholm et al., 1979, 1980). The first really important results were obtained in 1982 when magnetic susceptibility measurements showed that copper orders antiferromagnetically below the Néel temperature $T_{\mathrm{N}} = 58$ nK (Huiku and Loponen, 1982). In 1984, three antiferromagnetic phases were discovered in a single crystal specimen below the critical field $B_c = 0.25$ mT (Huiku et al., 1984, 1986).

In order to investigate, in more detail, the antiferromagnetically ordered spin structures of copper, neutron diffraction experiments were initiated in 1985 by a collaboration between the Risø National Laboratory in Denmark (Kurt Clausen and Per-Anker Lindgård), the Hahn–Meitner Institut in Berlin and the University of Mainz (Michael Steiner), and the Low Temperature Laboratory in Helsinki (Olli Lounasmaa). These measurements, carried out in Risø, extended by an order of magnitude the temperature regime at which neutron diffraction had been employed previously. In 1987, the first results were obtained when the (1,0,0) Bragg reflection was observed in copper confirming, indeed, antiferromagnetic order (Jyrkkiö et al., 1988). In 1989 another Bragg reflection, at $(1, \frac{1}{3}, \frac{1}{3})$, was found (Annila et al., 1990, 1992). The three antiferromagnetic phases, discovered by susceptibility measurements, were reproduced.

The work on silver started in Helsinki in 1987 (Oja et al., 1990). By employing magnetic susceptibility measurements, positive and negative spin temperatures of 0.8 nK and -4.3 nK were recorded. In the middle of 1990, antiferromagnetic order was found below 560 pK at positive temperatures (Hakonen et al., 1991). And, in 1991, the ferromagnetically ordered spin structure at negative temperatures was observed in silver, with ordering at $T_{\mathrm{C}} = -1.9$ nK (Hakonen et al., 1992). In 1993 the Danish-Finnish-German team started preparations for neutron diffraction work at $T > 0$ on silver at the Hahn–Meitner Institut in Berlin. In 1995 the antiferromagnetic Bragg peak at $(0, 0, 1)$ was seen (Tuoriniemi et al., 1995). A structure with the ordering vector $\mathbf{k} = (\pi/a)(0, 0, 1)$ developed when the ordered phase was entered by adiabatic demagnetization along the $[0, 0, 1]$ axis. The observed Bragg peak proves decisively spontaneous antiferromagnetic nuclear spin ordering in silver at $T > 0$. So far the neutron diffraction work has not been extended to negative spin temperatures, but such experiments should be technically feasible.

In rhodium, spin temperatures of 280 pK and -750 pK were produced in 1993 (Hakonen et al., 1993). These are the current world records on each side of the absolute zero. Spontaneous magnetic ordering has not been seen in rhodium so far.

The present paper is very short on theory but a comprehensive review (Oja and Lounasmaa, 1997), including an extensive theoretical section, will appear in the

January 1997 issue of Reviews of Modern Physics. I also refer to short articles by Hakonen et al. (1991) and by Hakonen and Lounasmaa (1994). I discuss the theory and practice of neutron diffraction experiments only very briefly (see the begining of Sect. 8); for a more complete treatment the publications by Steiner (1993) and by Nummila et al. (1997) should be consulted.

2 Theoretical remarks

Nuclear spins in metals provide good models to investigate magnetism. The nuclei are well localized, their spins are isolated from the electronic and lattice degrees of freedom at low temperatures, and the interactions between nuclei can often be calculated from first principles. Therefore, these systems are particularly suitable for testing theory against experiments. Comparisons with ab initio calculations allow rather deep new insights into the interactions leading to spontaneous nuclear ordering.

The Hamiltonian of the nuclear spin system can be written

$$H = H_{\rm dip} + H_{\rm RK} + H_Z + H_{\rm psd}\,. \tag{3}$$

In this expression the dipolar force between the magnetic moments of the nuclei is given by

$$H_{\rm dip} = \frac{\mu_0\hbar^2}{4\pi}\sum_{i<j}\gamma_i\gamma_j r_{ij}^{-3}\left[\mathbf{I}_i\cdot\mathbf{I}_j - 3r_{ij}^{-2}(\mathbf{r}_{ij}\cdot\mathbf{I}_i)(\mathbf{r}_{ij}\cdot\mathbf{I}_j)\right]. \tag{4}$$

The form of the dipolar interaction is known exactly. In Eq. (4), μ_0 is the permeability of free space, $\hbar$ is Planck's constant divided by 2π, γ is the gyromagnetic ratio (proportional to the nuclear magnetic moment μ), r_{ij} is the distance between spins i and j, and $\mathbf{I}$ is the nuclear spin. The appearance of the lattice vector $\mathbf{r}_{ij}$ in the second term in braces shows that the dipolar force is direction dependent, i.e., the interaction is anisotropic.

The so-called Ruderman–Kittel (1954) exchange force, caused by polarization of conduction electrons by the magnetic nuclei, is given by

$$H_{\rm RK} = -\sum_{i<j} J_{ij}(r_{ij})\,\mathbf{I}_i\cdot\mathbf{I}_j\,,$$

where

$$J(x) \propto [\cos x - (\sin x)/x]/x^3\,. \tag{5}$$

The expression for $H_{\rm RK}$ shows that the RK-force is isotropic. Calculations of $H_{\rm RK}$ requires detailed knowledge of the electronic band structure of the metal. The form

function $J_{ij}(r_{ij})$ is expanded in Eq. (5) using the free-electron approximation, but it has been calculated for copper and silver from first principles (Lindgård et al., 1986; Harmon et al., 1992). The RK exchange interaction, which oscillates with distance between neighbouring nuclei, can be ferro- or antiferromagnetic, depending on the lattice parameter and crystal symmetry.

The Zeeman interaction with the external magnetic field B is

$$H_Z = -\hbar\gamma \mathbf{B} \cdot \sum_i \mathbf{I}_i \,. \tag{6}$$

In copper, the ferromagnetic dipolar force is almost equal to the antiferromagnetic Ruderman–Kittel interaction, whereas in silver the latter dominates by a factor of 2.5. This leads to a complicated magnetic phase diagram (see Sects. 7 and 8) in Cu. Owing to the strong exchange force, the spin system in silver bears a close resemblance to an fcc Heisenberg antiferromagnet which has been the object of much theoretical interest owing to "frustration" (Binder and Young, 1986). With ferromagnetic forces between neighbours, there is no problem. Because the nuclear spin $I = 1/2$ in silver and rhodium, quantum effects are expected to be prominent.

In rhodium the *d*-electron-mediated anisotropic exchange forces, characteristic of transition metals, contribute as well (Bloembergen and Rowland, 1955). These can be taken into account, approximately, by a pseudodipolar term

$$H_{\mathrm{psd}} = \sum_{i<j} B_{ij}[\mathbf{I}_i \cdot \mathbf{I}_j - 3r_{ij}^{-2}(\mathbf{r}_{ij} \cdot \mathbf{I}_i)(\mathbf{r}_{ij} \cdot \mathbf{I}_j)] \tag{7}$$

in the Hamiltonian of Eq. (3).

Nuclear ordering in scandium metal has been investigated by Suzuki and his coworkers (Koike et al., 1995); they claim to have seen the transition to an ordered phase but the experimental data so far are not convincing. Pobell and his group at Bayreuth have studied thallium metal (Schröder-Smeibidl et al., 1991) and the cubic intermetallic compound $AuIn_2$; in these two substances the spin–lattice relaxation time is so short that conduction electrons and the nuclei are always in thermal equilibrium with each other. Recent data (Herrmannsdörfer et al., 1995) on $AuIn_2$ show that the ^{115}In nuclei order ferromagnetically at the surprisingly high Curie temperature $T_C = 35\ \mu$K. For a discussion of hyperfine enhanced materials, such as $PrNi_5$, I refer to Andres and Lounasmaa (1982).

All experiments on insulators, by Abragam, Goldman, and their coworkers (Bouffard et al., 1994) and by Wenckebach and his team (Van der Zon et al., 1990), have been performed using dynamic nuclear polarization, followed by adiabatic demagnetization in the rotating frame. The main weakness of the dynamic method of cooling is the inevitable presence of electronic paramagnetic impurities, introduced purposely to polarize the nuclei by the "solid effect"; the strong local

fields produced by the impurities probably blur, to a certain extent, some of the features of the nuclear long-range order. Copper, silver, and rhodium provide more general systems for experimental and theoretical studies of nuclear magnetism at positive and negative spin temperatures. These metals can be cooled by the brute force adiabatic nuclear demagnetization technique, without recourse to electronic impurities.

3 Negative spin temperatures

Much of the theoretical discussion in this section is based on the early work of Ramsey (1956) and Van Vleck (1957).

Energy level diagram for an assembly of silver or rhodium nuclei, at positive and negative spin temperatures, is shown schematically in Fig. 1; the spin $I = 1/2$,

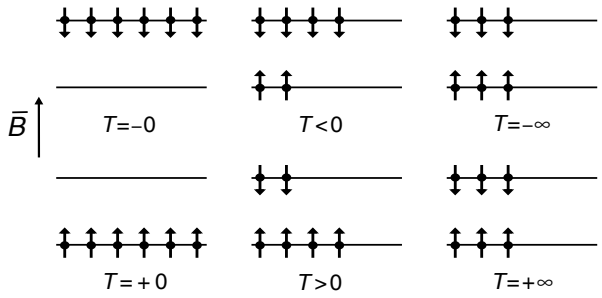

Figure 1. Energy-level diagram of nuclear spins in silver or rhodium at selected temperatures when B = constant (Hakonen and Lounasmaa, 1994).

so there are just two levels, corresponding to $\boldsymbol{\mu}$ parallel and antiparallel to the external field $\mathbf{B}$.

The distribution of the nuclei among the Zeeman energy levels is determined by the Boltzmann factor,

$$\exp(-\varepsilon/k_B T) = \exp(\boldsymbol{\mu} \cdot \mathbf{B}/k_B T)\,. \tag{8}$$

At positive temperatures the number of nuclei in the upper level, with $\boldsymbol{\mu}$ antiparallel to $\mathbf{B}$, is always smaller than in the lower level. At the absolute zero, all nuclei are in the ground state with $\boldsymbol{\mu}$ parallel to the external magnetic field $\mathbf{B}$. At $T < 0$ there are more spins in the upper than in the lower level.

Ordinarily, the temperature describes the average energy which is either connected with the free motion of the particles or with their vibrations about the lattice sites. In both cases the energy per particle is on the order of $k_B T$. The kinetic energy has no upper bound. Thus, if the temperature were raised towards infinity, the energy of the system would increase without limit. This is an unphysical situation and means that conduction electrons and the crystalline lattice cannot be brought to $T = \pm\infty$, even less to $T < 0$.

Negative temperatures, however, are possible when the energies of the particles are bound from above. In such cases, the absolute temperature is closely connected with the amount of disorder, i.e., with entropy. Let us consider nuclei in a constant external field $\mathbf{B}$. The magnetic moment $\boldsymbol{\mu}$ of each nucleus tends to orient itself along the field, but thermal motion produces disorder. When the temperature approaches zero, the entropy decreases. At $T = +0$, this causes complete order among the nuclei. In principle, one can also remove the nuclear disorder and approach the absolute zero from the opposite, negative side, $T \to -0$, by having the nuclear moments fully aligned antiparallel to the external field.

The theorems and procedures of statistical mechanics, such as the use of the partition function and the quantum mechanical density matrix, apply equally to systems at negative temperatures. By examining the statistical theory by which the Boltzmann distribution is derived, there is nothing objectionable a priori for the parameter $1/k_B T$ being negative; $T < 0$ simply means that the mean energy of the system is higher, instead of being lower than the energy corresponding to equal populations among the energy levels at $T = \pm\infty$.

The thermodynamic functions can be computed from the partition function, given for a 2-level system, with energy $\varepsilon = \pm\mu B$ (see Fig. 1), by the expression

$$Z = [\exp(\mu B/k_B T) - \exp(-\mu B/k_B T)]^N = [2\sinh(\mu B/k_B T)]^N \,, \tag{9}$$

where N is the number of spins in the assembly. Polarization p and entropy S are given by the relations

$$p = \tanh(\mu B/k_B T) \,, \tag{10}$$

$$S/R = \ln 2 - \tfrac{1}{2}[(1+p)\ln(1+p) + (1-p)\ln(1-p)] \,. \tag{11}$$

The thermodynamic quantities are functions of B/T only.

Near the absolute zero, $1/T$ or $\log T$ is sometimes used as the temperature function but, when $T < 0$, $\log T$ is not suitable. However, on the inverse-negative scale $\beta = -1/T$, the coldest temperature, $T = +0$, corresponds to $\beta = -\infty$ and the hottest temperature, $T = -0$, to $\beta = +\infty$. On this scale the algebraic order of β and the order from cold to hot are identical; the system passes from positive to negative Kelvin temperatures through $\beta = -0 \to +0$. The choice, $\beta = -1/T$, ensures that a colder temperature is always to the left side of a hotter one along the β-axis.

This inverse-negative scale thus runs in an "orderly" fashion from the coldest to the hottest temperature. The third law of thermodynamics appears "naturally" by the impossibility to reach the positive or negative ends of the β-axis infinitely far.

Figure 2 illustrates the entropy S, the specific heat at constant field C_B, and the internal energy U, suitably normalized, of a two-level spin assembly as a function of $\beta = -1/T$. The external field B and the energy level separation $2\mu B$ are

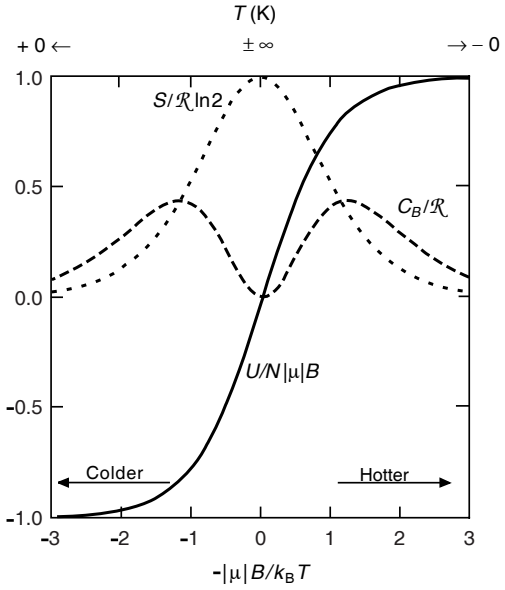

Figure 2. Entropy (dotted curve), internal energy (full curve), and specific heat (dashed curve) plotted as a function of $-|\mu|B/k_BT$ at B = constant for a nuclear spin system of two energy levels separated by $2\mu B$ ($I = 1/2$, $|\mu| = \frac{1}{2}\hbar|\gamma|$, and R is the gas constant).

assumed constant. The entropy has its maximum value $S = R\ln 2$ at $\beta = \pm 0$, i.e. at $T = -\infty$ or $T = +\infty$, because both energy levels are equally populated and polarization is zero. The specific heat C_B is zero at $\beta = -\infty$ and at $\beta = +\infty$ since all spins occupy their lowest or highest energy level at $T = \pm 0$ and no more heat can be removed or absorbed, respectively. At $\beta = \pm 0$, $C_B = 0$ as well because a very large change in T corresponds to a very small change in the spin configuration. The internal energy U has its lowest value at $T = +0$ and its highest value when

$T = -0$.

At $T < 0$, adiabatic demagnetization heats the spin system, instead of cooling it as happens when $T > 0$. Similarly, for experiments on polarized nuclei, at $T < 0$ the spin system must be heated to the hottest negative temperature to achieve maximum polarization, while at positive temperatures the spins must be cooled.

From the thermodynamic point of view, an essential requirement for the existence of a negative temperature is that the entropy S is not a monotonically increasing function of the internal energy U. In fact, whenever $(\partial S/\partial U)_B < 0$, $T = 1/(\partial S/\partial U)_B < 0$ as well. It was mentioned already that for negative temperatures to occur, there must be an upper limit to all allowed energy states of the system, otherwise the Boltzmann factor of Eq. (8) does not converge for $T < 0$. Nuclear spins satisfy this requirement since there are $2I + 1$ Zeeman levels and, indeed, $(\partial S/\partial U)_B$ changes sign at $T = \pm\infty$.

In addition, the elements of the spin assembly must, of course, be in internal thermodynamic equilibrium so that the system can be described by the Boltzmann distribution and thereby assigned a temperature. The thermal equilibrium time τ_2 among the nuclear spins themselves must be short compared to the time τ_1 of appreciable "leakage" of energy to or from other systems. In silver, for example, $\tau_1 = 28$ h at $T_e = 100$ μK, while $\tau_2 = 10$ ms.

We now return to the nuclear energy level diagram of Fig. 1. As the temperature is increased from $T = +0$, nuclei flip into the upper energy level and, at $T = +\infty$, there is an equal number of spins in both levels; the infinite temperature, however, does not cause any problems in this case since the energy spectrum has an upper bound. When the energy is increased further by lifting more spins to the higher level, the inversed spin distribution can still be described by the Boltzmann factor, see Eq. (8), but now with a negative temperature. Finally, when approaching the absolute zero from the negative side, $T \to -0$, eventually only the upper energy level is populated. Since heat is transferred from the warmer to the colder body when two systems are brought into thermal contact, negative temperatures are actually "hotter" than positive ones.

At $T = +0$, an isolated nuclear spin assembly has the lowest and, at $T = -0$, the highest possible energy. This important fact can be put on a more general basis. During demagnetization, the external magnetic field B at first completely controls the nuclear spin system. Entropy, a function of B/T, stays constant. However, when the field has been reduced sufficiently, approaching the internal local field B_{loc}, 0.25 mT in copper and 35 μT in silver and rhodium, the dipole–dipole and exchange forces gradually take over and the spin order begins to change from that forced by $\boldsymbol{B}$ to an arrangement determined by mutual interactions. During this spontaneous adjustment of spins the entropy increases, according to the general principles governing thermodynamic equilibrium, until S reaches a maximum while

the magnetic enthalpy

$$H = U - BM\,, \tag{12}$$

where M is the magnetization, stays constant because the system is isolated. If the entropy does not exceed a critical value, about 45% of its maximum $R\ln(2I+1)$, spontaneous spin order will occur.

In order to find the equilibrium spin configuration, one has to consider the variation of entropy under the restriction of a constant enthalpy, i.e., one must seek an extremum of $S + \lambda H$ where, by differentiation, Lagrange's multiplier $\lambda = -dS/dH = -1/T$. Therefore, one obtains $S - H/T = -G/T$ for the thermodynamic potential reaching an extremum; G is the Gibbs free energy. When temperature is positive,

$$G = H - TS \tag{13}$$

and the extremum is a minimum since S assumes its largest value at equilibrium. When the temperature is negative,

$$G = H + |T|S \tag{14}$$

and the Gibbs free energy obviously reaches a maximum.

The tendency to maximize the energy, instead of minimizing it, is the basic difference between negative and positive temperatures. In silver, the nearest-neighbour antiferromagnetic Ruderman–Kittel exchange interaction, three times stronger than the dipolar force, favours antiparallel alignment of the nuclear magnetic moments and thus leads to antiferromagnetism at positive spin temperatures. At $T < 0$, since the Gibbs free energy now must be maximized, the very same interactions tend to produce ferromagnetic nuclear order. This has been observed in experiments (see Sect. 9).

4 Achieving population inversion in practice

The Helsinki group has produced negative spin temperatures in silver and rhodium (see Sects. 9 and 11). In these metals, the spin–spin relaxation time $\tau_2 = 10$ ms; therefore, the nuclei can quickly equilibrate among themselves to a common spin temperature. On time scales 10 ms $\ll t \ll$ 10 h, two separate temperatures exist: one, T_e for the lattice and conduction electrons, and another, T for the nuclei. The spin–lattice relaxation time, $\tau_1 = (10\ \mathrm{sK})/T_e$ in silver and rhodium, is inversely proportional to the conduction electron temperature, see Eq. (2). For good thermal isolation between electrons and nuclei, a low T_e is thus needed; this is why the experiments must be carried out at ultra low temperatures.

Population inversion from positive to negative spin temperatures is rather hard to generate in metallic samples for two reasons: First, substantial effort is needed

to reach the high initial spin polarizations, and second, eddy currents make the production of inverted spin populations a difficult task. In spite of these problems, a team in Helsinki (Oja et al., 1990) decided to try such an experiment on silver: A small external magnetic field was reversed quickly, in about 1 ms, so that the nuclei had no chance to rearrange themselves among the energy levels.

This simple idea worked: Negative temperatures were produced in the nuclear spin system of silver but the loss of polarization was large. After improvements and refinements of the technique, fully satisfactory results were obtained; first on silver (Hakonen et al., 1990) and later on rhodium (Hakonen et al., 1993). In copper, $\tau_2 = 0.1$ ms, 100 times shorter than in silver and rhodium. Therefore, production of negative temperatures has not succeeded in copper, because the external magnetic field could not be reversed fast enough without causing massive eddy current heating in the specimen.

Indeed, it is important to realize that the field flip must be rapid in comparison to τ_2, the Larmor period of the spins in the local field B_{loc}. If this condition is not met, the spins are able to follow adiabatically the field reversal, and negative temperatures will not result. Demagnetization will just be followed by remagnetization to the positive starting temperature. In fact, during the quick field flip the Boltzmann distribution of the spins breaks down and, for a short moment, the system cannot be assigned a temperature. In a certain sense, the spin assembly passes from positive to negative temperatures via $T = +\infty \rightarrow -\infty$, without crossing the absolute zero. Therefore, the third law of thermodynamics is not violated. The needed increase in the energy of the spin system is supplied by the external magnetic field.

The rapid reversal of a small magnetic field, typically 400–500 μT, always resulted in a loss of polarization, i.e. increase of entropy of the spin system. The inversion efficiency from p_1 to p_2 was about 95% at small polarizations but decreased to 80% for $p_1 > 0.8$. Therefore, the studies at $T < 0$ in silver were limited to negative polarizations up to $p_2 \approx -0.6$.

The increase of entropy is, at least partially, explained by the heat that must flow to the spin–spin interaction "reservoir" to warm it to a negative temperature after population inversion, which reverses only the sign of the Zeeman temperature T_{Z} (Oja et al., 1990). Owing to the magnetic dipolar forces between the spins and other interactions, the Zeeman levels actually form bands which have an energy distribution and a temperature T_{ss} of their own.

Contrary to the Zeeman energy, the spin–spin interaction energy does not depend on B. By changing the external magnetic field, a difference can thus be produced between T_{Z} and T_{ss}. When B is much higher than B_{loc} (35 μT in silver), the separation of the two Zeeman energy levels is large in comparison with the width of the spin–spin bands. This means that the latter system has a very small

possibility to absorb an energy quantum produced when a spin is flipped. It then takes a long time for T_Z and T_{ss} to equalize. When $B \approx B_{loc}$, equilibrium is reached quickly. This process, leading to $T = T_Z = T_{ss}$, is probably an important reason for the polarization loss during the field reversal.

Before the field flip, $T_Z = T_{ss} = 10$ nK. After the 400 μT field is quickly reversed to -400 μT, $T_Z \approx -10$ nK but T_{ss} first stays at $+10$ nK. Since $B \gg B_{loc}$, the heat capacity of the Zeeman reservoir is much larger than the heat content of the spin–spin system, which guarantees that, after equilibrium, the spin temperature $T < 0$, but "colder" than -10 nK. As soon as $B \approx B_{loc}$, dipole–dipole and exchange interactions become important and, at the Curie temperature $T_C = -1.9$ nK, produce ferromagnetic order in silver (see Sect. 9).

5 Cryogenic techniques

To obtain nuclear temperatures in the nano- and picokelvin regimes, a sophisticated "brute force" cooling apparatus, with two nuclear refrigeration stages in series, has been employed in Helsinki, Risø and Berlin. The cryostats have, of course, undergone many important changes over the years. Precooling is done by a dilution refrigerator, and the large first nuclear stages have been manufactured from copper rods weighing over 1 kg. The second nuclear stage is the sample itself, made of a 2 g piece of bulk copper or of many 25 to 75 μm thick strips of silver or rhodium.

The specimen is connected to the precooling first nuclear stage without a heat switch. This means that the conduction electron temperature T_e is the same in both nuclear stages and that, for thermal isolation of the nuclear spin system in the sample, one relies entirely on the slowness of the spin–lattice relaxation process. The latest of these cascade nuclear refrigerators, operating at the Hahn–Meitner Institut in Berlin, is illustrated in Fig. 3. Cooling techniques below 1 K are discussed in detail by Lounasmaa (1974).

In copper the spin–lattice relaxation time is too short for experimental convenience, but for silver and rhodium τ_1 is inconveniently long, 28 h at 100 μK in a high magnetic field. Therefore, precooling a silver sample to 50 μK is a tedious process requiring two days. Owing to the limited capacity of the liquid ^{4}He bath, it was not feasible in the experiments on silver to wait long enough; this frequently prevented the use of starting temperatures lower than 100 μK.

Figure 4 is a schematic illustration, on a temperature vs. entropy diagram, of the procedure for cooling an assembly of silver or rhodium nuclei to negative nanokelvin temperatures. Numerical values refer to the YKI cryostat in Helsinki. One proceeds as follows:

- (A $\rightarrow$ B) Both nuclear stages are cooled to 10 mK by the dilution refrigera-

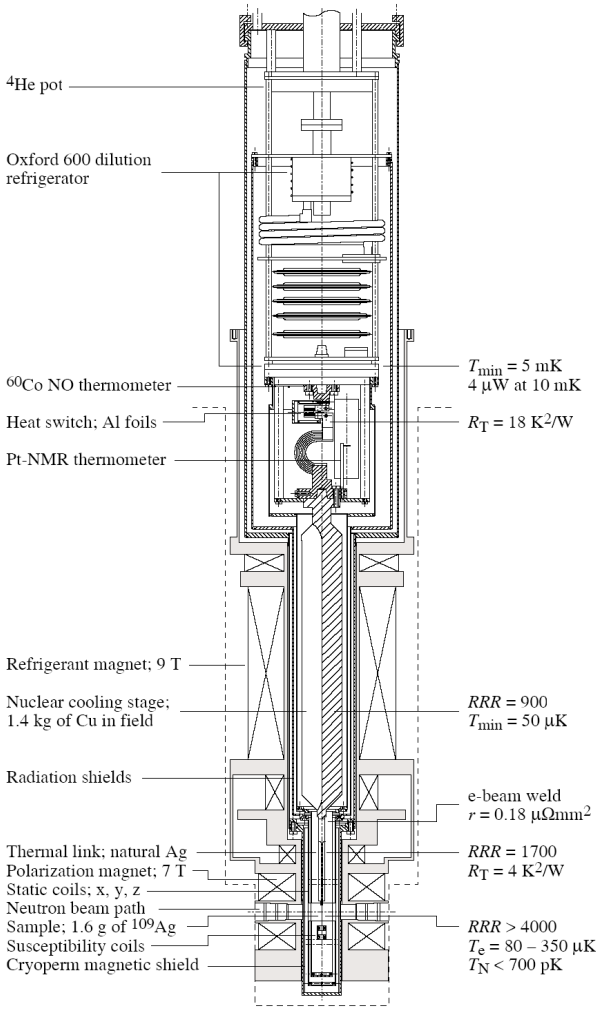

Figure 3. Cascade nuclear demagnetization cryostat designed for neutron scattering experiments on silver in Berlin (Nummila et al., 1997). The apparatus has a 9 T magnet surrounding the 1.4 kg copper nuclear cooling stage and a 7 T magnet for the sample. The copper refrigerant, demagnetized to 60 mT, keeps the lattice temperature at about 100 μK while the ^{109}Ag nuclei are polarized to 95%. The spins are further cooled into the picokelvin range by reducing the 7 T external field to zero. Before the end of demagnetization, an additional field of 400–500 μT is applied on the sample by a set of small coils, so that the ordered state can later be entered from any field direction. The Oxford 600 dilution refrigerator has a cooling power of 4 μW at 10 mK.

tor and, simultaneously, the nuclei in the first stage are polarized in a strong magnetic field of 8 T.

- (B → C) The first stage, made of 1400 g of copper, is adiabatically demagnetized to 100 mT, which produces a low temperature of ≈ 100 μK. Towards the end of demagnetization, the second nuclear stage, i.e. the sample, is magnetized to 8 T.

- (B → D) The 2 g silver or rhodium specimen of thin foils then slowly cools, in the high magnetic field of 8 T, by thermal conduction to ≈ 100 μK.

- (D → E) As the next step, the sample is adiabatically demagnetized from 8 T to 400 μT, whereby the spins reach approximately 10 nK. They are thermally isolated by the 28 h spin–lattice relaxation process from the conduction electrons which are anchored to 100 μK by the first nuclear stage at C.

- (E → F) Finally, the negative spin temperature is produced in the system of silver or rhodium nuclei by reversing the 400 μT magnetic field in about 1 ms. The increase in the energy of the spin system is absorbed from the external magnetic field. The rapid inversion causes some loss of polarization, i.e. increase of entropy. By continuing demagnetization to $B = 0$, the record temperature of −750 pK was reached in rhodium. In silver, dipole–dipole and exchange interactions produced ferromagnetic order at the Curie temperature $T_{\mathrm{C}} = -1.9$ nK.

- (F → G → A) The system then begins to lose its negative polarization, crossing in a few hours, via infinity, from negative to positive temperatures. The measurements must be carried out in about 10–30 min after the final demagnetization, since the nuclear spin temperature starts immediately to relax towards $T_e = 100$ μK with the time constant τ_1, determined by the spin–lattice relaxation process.

- (C → A) The first nuclear stage warms slowly, under the 100 mT field, from 100 μK towards 15 mK. A new experimental sequence can then be started.

If production of negative spin temperatures was not intended, demagnetization from 400 μT was continued at E to zero field, resulting in the record temperature of 280 pK in rhodium. In silver, dipole–dipole and exchange interactions produced antiferromagnetic order at the Néel temperature $T_{\mathrm{N}} = 560$ pK.

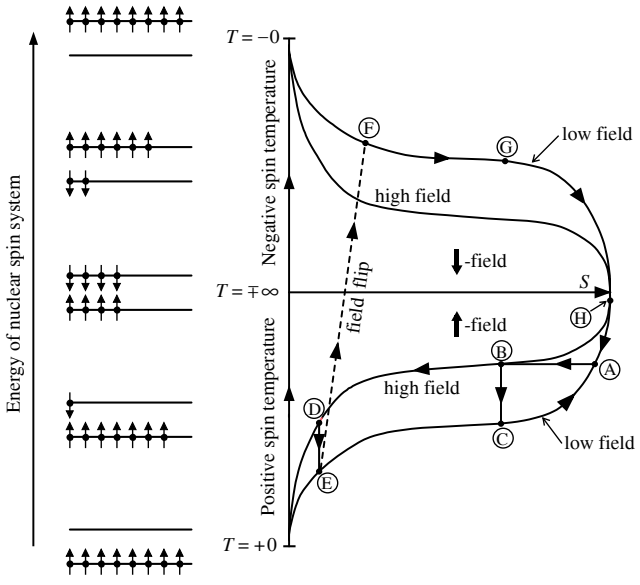

Figure 4. Schematic illustration of the cascade nuclear cooling process to produce negative spin temperatures (Lounasmaa et al., 1994).

6 Measurement of spin temperature

One of the difficult tasks in these experiments was to measure the absolute temperature of the thermally isolated nuclei. The usual technique employs directly the second law of thermodynamics, viz.

$$T = \Delta Q / \Delta S \,. \tag{15}$$

At positive temperatures, the nuclear spin system is supplied with a small amount of heat ΔQ and the ensuing entropy increase ΔS is calculated from the measured loss of nuclear polarization (see below). The method works equally well at negative spin temperatures: $\Delta Q < 0$ when entropy increases. The system radiates some of its energy at the nuclear Larmor frequency while the populations of the two energy levels tend to equalize.

The primary observable in these experiments is the nuclear magnetic resonance signal (Slichter, 1990), recorded by a SQUID. We measured $\chi(\nu) = \chi'(\nu) + i\chi''(\nu)$ using frequency sweeps across the resonance in a constant magnetic field. This was done at low frequencies where the skin effect does not prevent the magnetic field from penetrating into the metalic specimen. The experimental setup for recording

the susceptibility has evolved over the years. One of the later SQUID-NMR systems is described by Hakonen et al. (1993).

From χ'', applying the Kramers–Kronig relation

$$\chi'(0) = (2/\pi) \int (\chi''(\nu)/\nu) d\nu \,, \tag{16}$$

one can calculate χ' which, at the low frequencies, is equal to the static susceptibility $\chi'(0)$; ν is the NMR excitation frequency. Furthermore, from the measured χ'' it is possible to deduce the nuclear polarization using the well known relationship

$$p = A \int \chi''(\nu) d\nu; \tag{17}$$

the proportionality constant A can be calibrated against the platinum-NMR temperature scale around 1 mK. Equation (17) is valid when $B \gg B_{\rm loc}$. When the polarization has been determined, one can compute the entropy, Eq. (11), because, at these ultralow temperatures, the only contribution to S is from the nuclear spins.

One of the drawbacks in measuring the nuclear temperature directly by means of the second law, Eq. (15), is that the applied ΔQ warms the spins substantially because a large heat pulse is needed to allow an accurate determination of ΔS. Only a small number, 7 to 9 points per run, could be obtained, but more data are needed for studies of ordering, which was revealed both by changes in the shape of the NMR line and by a plateau in the static susceptibility vs. time curve. For this reason, Hakonen et al. (1991) developed another method of thermometry by first investigating the connection between polarization and temperature. By equating the second order expansion of entropy in terms of polarization, viz.

$$S/R \ln 2 = 1 - p^2/(2 \ln 2) \,, \tag{18}$$

with the $1/T^2$-expansion of entropy, one obtains a linear dependency between $1/p$ and T. The low temperature end is also known approximately: By neglecting quantum fluctuations, one expects that $p \to 1$ when $T \to 0$. In fact, an almost linear relationship was found below $|T| < 10$ nK, namely

$$1/|p| - 1 = 0.55(|T|/\text{nK}), \tag{19}$$

both at $T > 0$ and $T < 0$. The accuracy of the measured temperatures is $\pm 20\%$.

During neutron diffraction experiments it is possible to employ the transmission of a polarized neutron beam as a primary thermometer. The paper by Lefmann et al. (1997) describes this convenient and accurate method in some detail. Even unpolarized neutrons can be used for absolute thermometry without calibration. An important advantage of neutron thermometry is that the technique can be applied in any magnetic field and on bulk metal samples, unlike the NMR method.

The neutron technique was used recently in studies of nuclear magnetic ordering of ^{109}Ag nuclei at nanokelvin temperatures (see Sect. 10). Transmission of thermal neutrons provided a convenient tool for monitoring the state and evolution of the spin assembly (Tuoriniemi et al., 1997).

7 Susceptibility measurements on copper

The Helsinki investigations of spontaneous nuclear magnetic ordering were started in the mid 1970's by constructing a two-stage nuclear demagnetization cryostat. Evidence for antiferromagnetic order in copper was found in 1978 (Ehnholm et al., 1979, 1980) but it took four years before magnetic susceptibility measurements showed that the actual transition is at $T_{\mathrm{N}} = 58$ nK (Huiku and Loponen, 1982). In two more years experiments were made using a single-crystal specimen (Huiku et al., 1984, 1986). By an elaborate coil system one could measure the susceptibility in all three Cartesian directions.

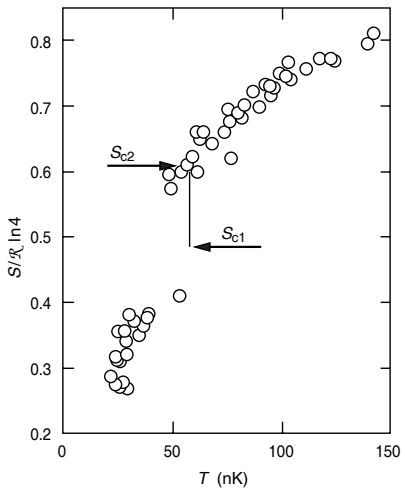

Figure 5. Reduced nuclear entropy $S/R\ln 4$ of copper vs. the spin temperature in nanokelvins (Huiku et al., 1986).

Figure 5 shows an important result, the spin entropy of copper; $S_{\max} = R\ln 4$ for Cu because the nuclear spin $I = 3/2$. There is a clear jump in entropy which

signifies a first order change to an antiferromagnetic phase. $T_{\rm N} = 58$ nK was, at the time, the lowest transition temperature ever observed or measured. S_{c1} is the lower and S_{c2} the higher critical entropy. This measurement was done on a polycrystalline copper sample.

Figure 6 illustrates the x-, y-, and z-components of the susceptibility in three external fields. For analyzing the data, one must first recall how the longitudinal and transverse susceptibilities behave below the Néel point in electronic antiferromagnets: $\chi_\perp$, the susceptibility transverse to sublattice magnetization, is constant while $\chi_\parallel$, the susceptibility parallel to sublattice magnetization, approaches zero as $T \to 0$. Consequently and by analogy, when $B = 0$, the magnetization is

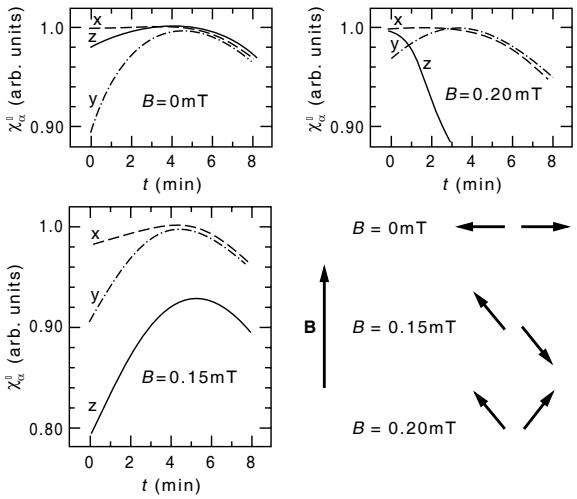

Figure 6. Susceptibility χ_α of a Cu single crystal, along the three Cartesian directions ($\alpha = x, y, z$) as a function of time in external fields $B = 0$, 0.15, and 0.20 mT. The originally suggested spin arrangements are illustrated in the lower right corner. The sample was a slab of dimensions $0.5 \times 5 \times 20$ mm^3 along the x-, y- and z-directions, respectively (Huiku et al., l986).

mainly along the y-axis since changes in χ are largest in this direction.

At $B = 0.15$ mT, the sublattice magnetization has its biggest component in the z-direction but it also has a smaller component in the y-direction. At $B =$ 0.20 mT, the spins are leaning towards the external magnetic field because there is no longer antiferromagnetism in the z-direction. Furthermore, in contrast to

the "paramagnetic" behaviour of χ_z, a small increase in χ_y indicates an antiferromagnetic y-component of magnetization. Since χ_x is approximately constant in all fields, the sublattice magnetization is always perpendicular to the x-direction. These characteristically different behaviours indicate three separate, antiferromagnetically ordered regions in the nuclear spin system of copper.

Figure 7 shows the B–S phase diagram of copper; it was constructed by demagnetizing from different initial values of entropy, between 10% and 35% of $R \ln 4$, i.e., by moving down on the diagram, and then by letting the specimen to warm up, thus moving horizontally to the right while the susceptibility was being measured. The low field phase is marked by AF1, the middle field phase by AF2, and the

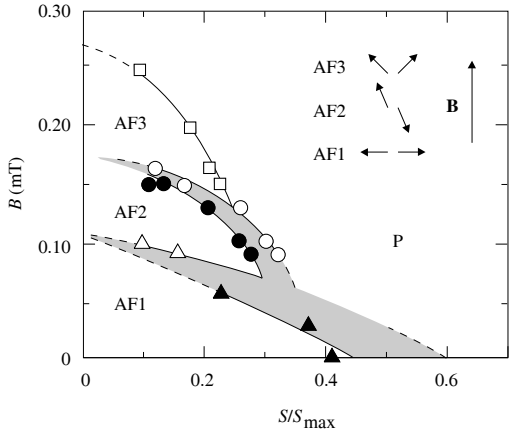

Figure 7. External magnetic field vs. entropy diagram of copper nuclear spins (Huiku et al., 1986). The critical field $B_c \approx 0.25$ mT. The Néel temperature $T_N \approx 60$ nK.

high field phase by AF3; the paramagnetic phase P is at right. The shaded regions indicate where one characteristic behaviour changes to another and a latent heat is being supplied; $\Delta S \approx 0.12 R \ln 4$. The spin arrangements are again drawn into the figure.

A phase diagram in the magnetic field vs. temperature plane was not constructed because temperatures could be measured reliably only in zero field. Nevertheless, surprisingly many interesting results were obtained from these simple but technically very difficult susceptibility measurements.

8 Neutron diffraction on copper

However, no detailed information about the ordered spin structures can be extracted from susceptibility data. The appropriate technique is neutron diffraction, which is the most powerful method for microscopic structural studies of magnetic systems because the neutron-nucleus scattering length a is spin dependent (Price and Sköld, 1986; Windsor, 1986; Steiner, 1990). The relevant equation is

$$a = b_0 + b\mathbf{I}\cdot\mathbf{S}\,, \tag{20}$$

where b_0 and b are constants, $I = 3/2$ is the nuclear spin of copper, and $S = 1/2$ is the spin of the neutron. The observed scattered neutron intensity is proportional to the square of the sublattice polarization. Likewise, the nuclear absorption cross section is also spin dependent. In both cases, the sensitivity is increased significantly by the use of a polarized beam.

Successful neutron diffraction experiments on copper were undertaken by a Danish-Finnish-German collaboration at the Risø National Laboratory in Denmark. Copper has an fcc structure which means that only reflections with all Miller indices (h, k, l) even or all odd are allowed. Long-range antiferromagnetic order in the nuclear spin system gives rise to additional Bragg peaks with (h, k, l) mixed, which yield the translational symmetry of the magnetic superstructure. However, nuclear scattering, which results from the strong interaction, but not from dipolar forces as in electronic neutron diffraction experiments, is isotropic in the spin space which makes it impossible to assign directions to the magnetic moments relative to the lattice axes. Polarized neutrons with a full polarization analysis would provide this information. So far, however, the magnetic shields (see Fig. 3), needed around the sample for the ordering experiments below $B_c \approx 0.25$ mT, depolarized the neutron beam in low fields.

In zero external magnetic field, theoretical calculations predicted antiferromagnetic structure (Lindgård, 1988), exemplified by the modulation vector $\mathbf{k} = (\pi/a)(1, 0, 0)$, which yields a (1,0,0) Bragg peak (Kjäldman and Kurkijärvi, 1979). In copper, the lattice constant $a = 3.61$ Å. In high fields, especially along the $[1, 1, 0]$ direction, a 3-**k** state, in which the modulation is a superposition of all three $\{1, 0, 0\}$ vectors, was predicted (Heinilä and Oja, 1993).

The experiments were carried out in the neutron guide hall next to the DR-3 reactor in Risø using a standard two-axis spectrometer (Jyrkkiö et al., 1988, 1989). A two-stage nuclear demagnetization cryostat, especially designed for studies of nuclear magnets by neutron diffraction, was constructed in Helsinki for these experiments. Instead of natural copper, which is an almost equal mixture of ^{63}Cu and ^{65}Cu and which was used in the susceptibility measurements (see Sect. 7), ^{65}Cu was chosen as the sample material because a factor of six is gained in the scattered

neutron intensity this way. Figure 8 shows a block diagram of the experimental arrangement. The neutron beam is first reflected by a graphite monochromator

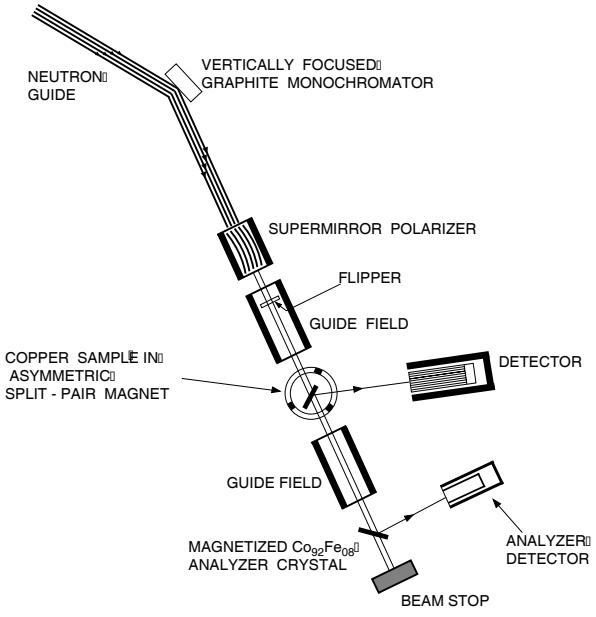

Figure 8. Neutron diffraction setup at Risø for studies of copper using a polarized beam (Jyrkkiö et al., 1988). The cryostat is mounted on the spectrometer turntable. Polarization of the beam is maintained by a constant vertical guide field of 1–2 mT outside the cryostat and by the large field of the asymmetric second stage magnet inside. The flipper coil is used to reverse the beam polarization. A typical flux at the site of the sample is $2 \cdot 10^5$ neutrons $\mathrm{cm}^{-2}\mathrm{s}^{-1}$.

crystal. It then passes through a supermirror polarizer and hits the sample in the cryostat; the scattered neutrons are counted by the detector and the beam polarization is measured from transmitted neutrons by the analyzer.

The cryostat, mounted on a turntable, and the detector attached to it could be moved independently in the scattering plane before an experiment was started. The sample must be positioned so that the particular plane in the reciprocal space, which is accessible to neutron diffraction measurements, contains the **k**-vectors of

the most probable spin structures in the magnetically ordered states. Because of the limited time available for experiments in the ordered state, a single crystal specimen is neccessary for a reasonable statistical accuracy. It should be noted that the external magnetic field during the initial neutron diffraction experiments on copper was in the $[0, -1, 1]$ direction of the crystal, whereas the susceptibility measurements in Helsinki were made with the field in the $[0, 0, 1]$ direction.

Heating caused by the neutron beam is, of course, a drawback in these experiments. The target nuclei are warmed mainly through processes following neutron capture, i.e. by prompt γ-rays and by β-emission from the radioactive intermediate nuclei. Much of the energy released by γ-radiation escapes since the penetration depth is typically a few centimeters; for thin specimens (< 1 mm) the fraction of the absorbed energy is usually less than 5%. In contrast, the charged β-particles dissipate their kinetic energy very effectively in solids; the fraction of β-energy absorbed is typically 50–80% of the total.

In the autumn of 1987, a clear antiferromagnetic (1,0,0) Bragg peak, characteristic of simple Type-I order in an fcc lattice, was observed below $T_{\mathrm{N}} = 60$ nK. The neutron intensity and the static longitudinal susceptibility $\chi_{\parallel}$, as functions of time after the field had been reduced to zero, are shown in Fig. 9. And there were, indeed, neutrons, and plenty of them during the first few minutes! Since the counter

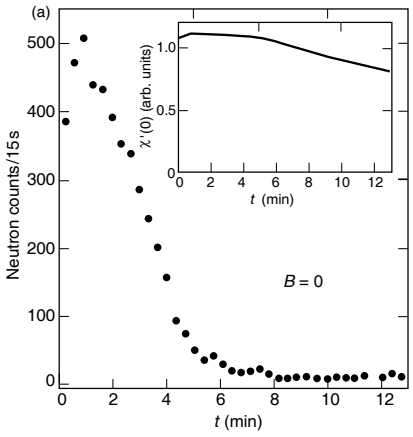

Figure 9. Neutron diffraction and susceptibility data on the nuclear spin system of copper (Jyrkkiö et al., 1988).

was in the $(1,0,0)$ Bragg position of mixed indices (h,k,l) antiferromagnetism in copper had been proven by the neutron diffraction data beyond all doubt!

During the first 4–5 min $\chi_{\parallel}$, illustrated in the insert of Fig. 9, showed almost a plateau, indicating an antiferromagnetic state; this agrees with the susceptibility experiments in Helsinki (see Fig. 6). The neutron signal displayed, for the first minute, a small increase. After this, during the susceptibility plateau, the neutron count diminished rapidly, indicating a fast decrease in the antiferromagnetic sublattice polarization as the nuclei warmed up owing to the spin–lattice relaxation process. The susceptibility settled to an exponential decrease, characteristic of the paramagnetic state, in about 7 min after the end of the final demagnetization. By this time the temperature had increased above $T_{\mathrm{N}} = 60$ nK and the remaining neutron signal had disappeared.

To obtain more information about the phase diagram of nuclearly ordered copper, intensities of scattered neutrons were measured at many non-zero fields. The data, showing variations of the neutron count and of the nuclear susceptibility as functions of time after reaching the final field, are presented in Fig. 10.

At $B = 0.04$ mT, the qualitative behaviour of the neutron count is similar to that at $B = 0$, but the intensity is less. The susceptibility, too, is similar in both fields. At $B = 0.08$ mT, the neutron intensity was further reduced; the susceptibility had a small maximum at 1 min, but it then reached a plateau and started to bend after 6 min towards its final paramagnetic behaviour. At $B = 0.10$ mT, the susceptibility shows, in contrast, a clear increase for the first 4 min, whereas the neutron intensity is almost zero during the entire experiment.

At $B = 0.12$ mT, the neutron data are drastically different from the results at lower fields. The intensity was very high immediately after the final field had been reached and showed no increase but a very rapid decrease at the beginning of the experiment; after about 2.5 min no neutron signal was observable. The susceptibility increased almost 20% during the first 4 min. The neutron count thus disappeared clearly before the system was at T_{N}, which was reached approximately at the susceptibility maximum.

At $B = 0.16$ mT the characteristics were similar to those at zero field. The neutron intensity was very high initially, as at $B = 0.12$ mT, but it now decreased much more slowly. The disappearance of the count was coexistent with the maximum of $\chi_{\parallel}$. The behaviour of the susceptibility was qualitatively the same as at $B = 0.10$ and 0.12 mT, showing first a clear increase. In still higher fields no drastic changes happened: At $B = 0.20$ and 0.24 mT, the neutron signal was qualitatively the same as at $B = 0.16$ mT, but the intensity was smaller, especially at 0.24 mT. The susceptibility increase at $B = 0.16$ mT was reduced to a plateau at $B = 0.20$ mT and at $B = 0.24$ mT, only a decreasing slope was observed. Finally, at $B = 0.30$ mT (not shown in Fig. 10), no signs of ordering were seen, neither in

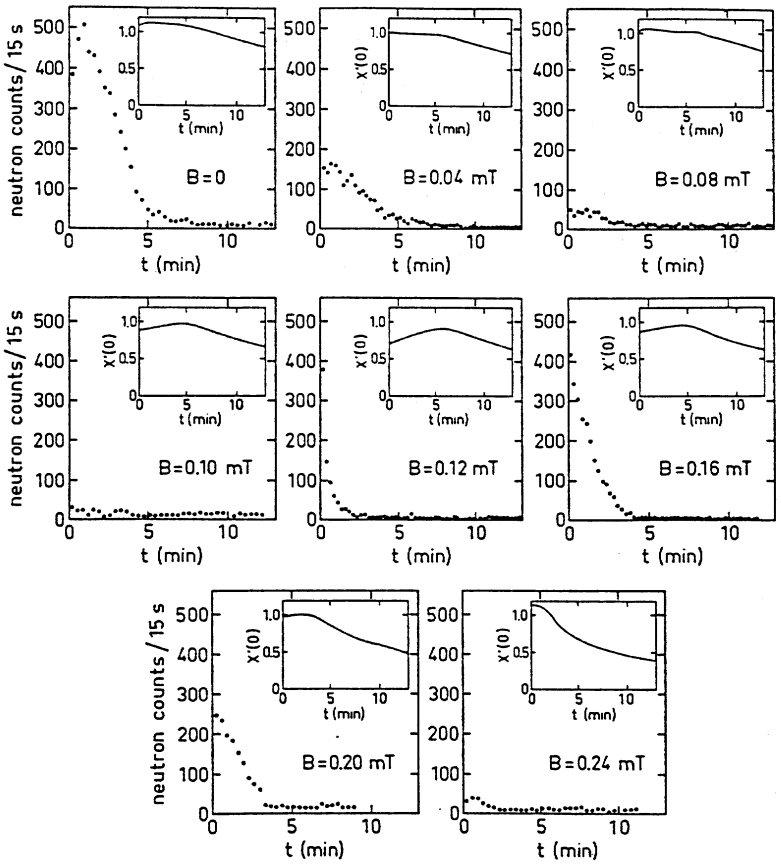

Figure 10. Integrated neutron intensity measured for copper at the (1,0,0) Bragg position and the static susceptibility $\chi'(0)$ (in arbitrary units) as functions of time after final demagnetization to the field indicated on each frame (Jyrkkiö et al., 1988).

the neutron intensity nor in the susceptibility signal.

The neutron data above $B \geq 0.16$ mT suggest that, at elevated fields, the nuclear spins tilt towards B and that, thereby, the contribution to the antiferromagnetic peak becomes weaker. By extrapolating to the field at which the neutron intensity disappeared, the critical field $B_c = 0.25$ mT was obtained; this value is the same as was observed in the susceptibility measurements (Huiku et al., 1986). The drastic change in the neutron intensity between $B = 0.08$ and 0.12 mT indicates a phase transition at about $B = 0.10$ mT.

The most interesting observation was that at the (1,0,0) Bragg reflection a lot of neutrons were seen in low fields and also in fields near 0.16 mT but that in-between, around 0.10 mT, there were very few scattered neutrons. At 0.12 mT many counts were recorded at first but the neutrons disappeared rapidly. The intriguing question was: What about neutrons of the in-between region, where the spins clearly were ordered according to susceptibility measurements?

So the Risø group decided to start looking at other positions in the reciprocal lattice for the missing neutron intensity. But this was not so easy! In conventional neutron diffraction experiments one can scan the reciprocal space automatically for days and observe the peaks as they go by, but in this case the total time available for measurements was about 5 min after demagnetization. And it took at least two days before the sample was ready again for the next experiment! So one had to think carefully where to look for the missing neutrons; it would have taken much too long to map out all regions of the reciprocal space. Fortunately, theoretical calculations by Lindgård (1988) helped in planning the experiments.

Success came in 1989 when four new but equivalent antiferromagnetic Bragg peaks, $(1, \frac{1}{3}, \frac{1}{3})$, $(1, -\frac{1}{3}, -\frac{1}{3})$, and $\pm(0, -\frac{2}{3}, -\frac{2}{3})$, were found (Annila et al., 1990, 1992). It was unexpected that the order proved to be simply commensurate with a three-sublattices structure, not observed previously in any fcc antiferromagnets. The discovery was made when the reciprocal lattice was searched along the high symmetry directions; this is the first time that conventional scanning was employed at nanokelvin temperatures.

From the neutron count vs. time curves an intensity contour diagram was constructed; the result is shown in Fig. 11. Three maxima were found: at $B = 0.09$ mT for the $(1, \frac{1}{3}, \frac{1}{3})$ reflection and at $B = 0$ and $B = 0.15$ mT for the $(1, 0, 0)$ reflection. The $(1, \frac{1}{3}, \frac{1}{3})$ signal was strongest when the (1,0,0) signal was weakest and vice versa, implying the presence of three distinct antiferromagnetic phases in copper. The neutron data are thus in excellent agreement with earlier susceptibility measurements (see Fig. 7). The reason for the rapid disappearance of the (1,0,0) neutron signal at 0.12 mT (see Fig. 10) was probably that the high field (1,0,0) phase, formed immediately after the field had been reduced to $B_{\mathrm{C}} = 0.25$ mT, was still changing to the $(1, \frac{1}{3}, \frac{1}{3})$ phase. A remarkable reature of the phase diagram of

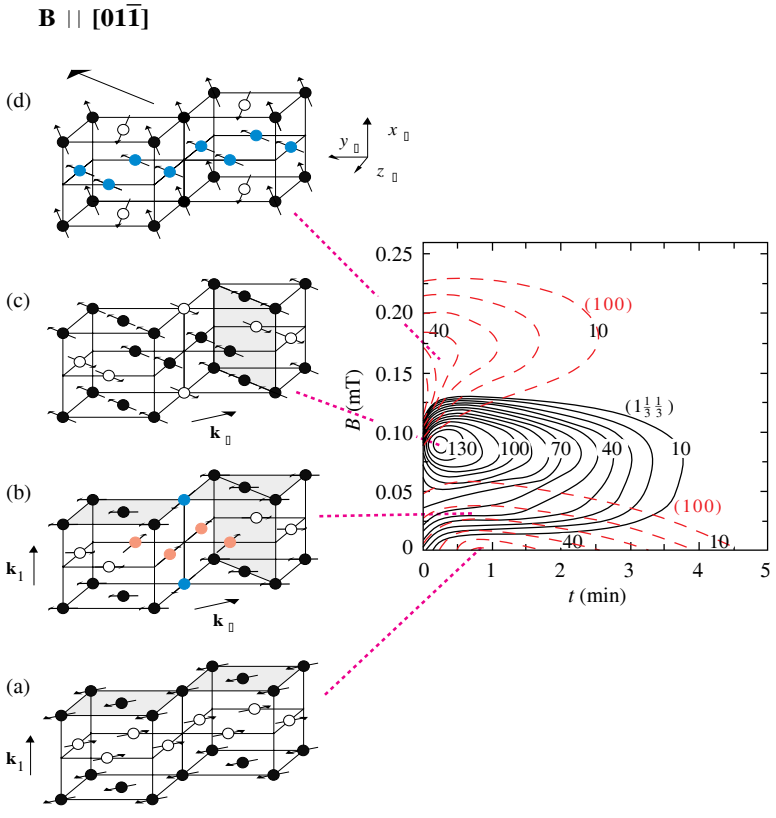

Figure 11. At right: Neutron intensity contour diagram of copper for the $(1, \frac{1}{3}, \frac{1}{3})$ (solid curves) and $(1, 0, 0)$ (dashed curves) Bragg reflections as functions of time (i.e. of temperature) and the external magnetic field. The number of neutrons collected per second is marked on the contours (Annila et al., 1990). At left: Spin structures of copper for the $[0, 1, -1]$ alignment of the magnetic field. (a) $B = 0$: antiferromagnetic $\mathbf{k}_1 = (\pi/a)(1, 0, 0)$ structure consisting of alternating ferromagnetic planes. (b) $0 < B < B_c/3$: Coexistence of structures with ordering vectors $\mathbf{k}_1 = (\pi/a)(1, 0, 0)$ and $\mathbf{k} = \pm(\pi/a)(0, \frac{2}{3}, \frac{2}{3})$, illustrated for $B = 0.17B_c$. The $(0, \frac{2}{3}, \frac{2}{3})$ and $(1, \frac{1}{3}, \frac{1}{3})$ reflections are equivalent under fcc symmetry. (c) $B = B_c/3$: Left-left-right structure with $\mathbf{k} = \pm(\pi/a)(0, \frac{2}{3}, \frac{2}{3})$ order. (d) High field configuration with three ordering vectors: $(\pi/a)(1, 0, 0)$, $(\pi/a)(0, 1, 0)$, and $(\pi/a)(0, 0, 1)$. The spin structures, which are consistent with the neutron diffraction data, were drawn according to theoretical calculations by Viertiö and Oja (1992).

copper is its complexity.

An obvious extension to the experiments described so far was to examine the phase diagram when the external magnetic field was aligned along the other main crystallographic axes, besides the $[0, -1, 1]$ direction. A number of very successful experiments were made at different field alignments in Risø (Annila et al., 1992). The observed antiferromagnetic states were bounded by the second order critical field line; the $B_c(T)$ curve was determined from the neutron diffraction and susceptibility data. In fields between 0.10 and 0.20 mT, the (1,0,0) order was strong over a wide span of directions around $\mathbf{B} \parallel [1, 0, 0]$ and over a narrower angular region about $\mathbf{B} \parallel [0, 1, 1]$. There was also pure (1,0,0) order near the origin in fields below 0.01 mT.

The susceptibility measurements in Helsinki were made along the $[0, 0, 1]$ field direction; the three phases, AF1, AF2, and AF3, predicted by the data (see Fig. 7), were reproduced by the experimental neutron diffraction results. The $(1, \frac{1}{3}, \frac{1}{3})$ phase had strong maxima around 0.07 mT, both in the $[1, 0, 0]$ and the $[0, 1, 1]$ field directions, but in between the intensity was somewhat less. The ordering vector for the $\mathbf{B} \parallel [1, 1, 1]$ direction was the main puzzle: There was a large antiferromagnetic region with no neutron intensity! In spite of considerable efforts to find a new Bragg reflection in this field direction, no neutrons were discovered.

In order to determine the spin structure from the neutron diffraction experiments one needs theoretical guidance. This is, as was mentioned already, because the scattering cross section, unfortunately, does not depend on the direction of the spins in relation to the crystalline axes; only the periodicity of the magnetic lattice can be deduced from neutron diffraction data on antiferromagnetically ordered nuclei. The anisotropic dipolar interaction is too weak to be of use because of the small nuclear magnetic moments. A successful calculation of the selection rules between the various antiferromagnetic phases in copper has been made by Viertiö and Oja (1992, 1993).

A thorough discussion of the many theoretical calculations, by Oja and his group (Oja and Viertiö, 1993; Viertiö and Oja, 1987, 1990, 1993; Heinilä and Oja, 1993, 1996), by Lindgård (Lindgård et al., 1986; Lindgård, 1988, 1992), and by Frisken and Miller (1986, 1988), is given in the long review of Oja and Lounasmaa (1997). A striking feature of the phase diagram of copper is the strong coexistence of the $(1, 0, 0)$ and $(1, \frac{1}{3}, \frac{1}{3})$ phases along the boundaries. A very clear time and history dependence accompanied every passage through the phase diagram. Oja and Lounasmaa (1997) discuss in detail the kinetics of the phase transitions in copper (see Sect. VII.F. of their review).

9 Susceptibility measurements on silver

The susceptibility measurements on silver, at positive and negative spin temperatures, were carried out in Helsinki (Oja et al., 1990; Hakonen et al., 1991, 1992). The magnetic moment μ of Ag nuclei is about 20 times smaller than that of copper, which means, since the dipolar interaction goes as μ^2, that more than two orders of magnitude lower transition temperatures are expected. Figure 12 illustrates the NMR absorption and emission spectra of silver nuclei measured at $T = 1.0$ nK and at $T = -4.3$ nK. The imaginary component of susceptibility χ'' has been plotted against the NMR frequency ν. The data show that instead of absorption, as at positive temperatures, the system is emitting energy at the Larmor frequency when the temperature is negative.

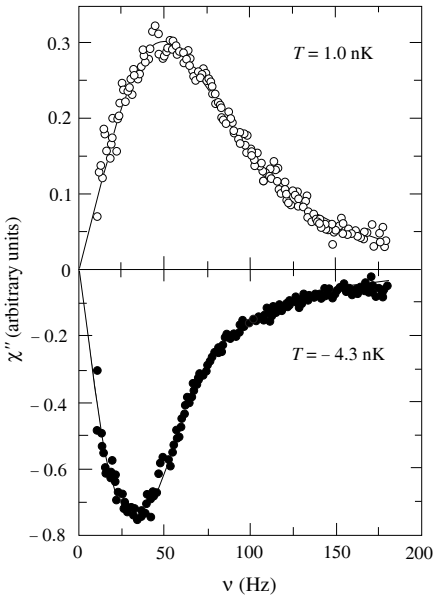

Figure 12. NMR absorption and emission spectra for silver, measured in zero magnetic field (Hakonen et al., 1990); solid curves are Lorentzian lineshapes. Note the different vertical scales for the $T = 1.0$ nK and $T = -4.3$ nK data.

In Fig. 13 the absolute value of the inverse magnetic susceptibility $|1/\chi'(0)|$ of silver, calculated from the Kramers–Kronig relation, see Eq. (16), is plotted as a

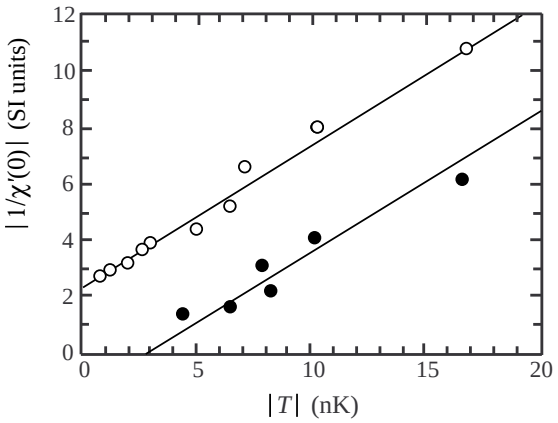

Figure 13. Absolute value of the inverse static susceptibility $|1/\chi'(0)|$ vs. absolute value of temperature for silver, measured at $T > 0$ (○) and at $T < 0$ (●) (Hakonen et al., 1990).

function of $|T|$ in nanokelvins. We note that at positive temperatures one obtains a straight line with an intercept on the left side of the $|1/\chi'(0)|$-axis. This behaviour is typical and indicates that silver tends to antiferromagnetic order when $T \to +0$. At negative temperatures the intercept is on the right side of the $|1/\chi'(0)|$-axis which shows that, when $T \to -0$, the spin system of silver nuclei prefer ferromagnetic order, as expected (see Sect. 3); the Néel and Curie points, however, were not reached in these first experiments. The data, both at $T > 0$ and at $T < 0$, followed the Curie–Weiss law

$$\chi = C/(T - \theta) \tag{21}$$

down to the lowest experimental temperatures.

Final success came in 1991. When the static susceptibility was measured as a function of time, a small maximum or, at least, a kink was seen. Such data, depicted in Fig. 14, showed that the nuclear spin system of silver had reached the antiferromagnetic state. In zero field, the measured Néel point was $T_{\mathrm{N}} = 560$ pK. This is the lowest transition temperature that has ever been recorded.

Subsequently, spontaneous nuclear order was produced at negative spin temperatures as well. This is shown in Fig. 15 which illustrates the static susceptibility of silver as a function of the nuclear spin polarization measured in zero field (○) and at a 5 μT field oriented perpendicular (△) and parallel (×) to the sample foils. The crossing of the two lines is identified as the transition point to the ferromagnetic

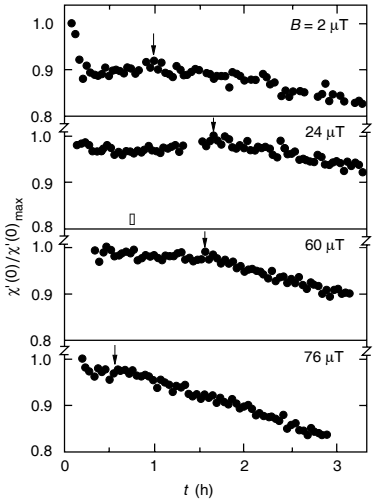

Figure 14. Static susceptibility $\chi'(0)$ of silver nuclei as a function of time after demagnetization to four different external magnetic fields (Hakonen et al., 1991). Each set of data is scaled by the maximum susceptibility $\chi'(0)_{\max}$ for that run. Small arrows indicate the transition point from the ordered to the paramagnetic phase.

state. Owing to the rounding of the $\chi(p)$ vs. p curve, one obtains for the critical polarization, in zero field and in 5 μT, the value $p_c = 0.49 \pm 0.05$ which corresponds to $S_c/(R \ln 2) = 0.82 \pm 0.035$.

At $B = 0$, the magnetic susceptibility of silver spins was found to saturate at $\chi_{\rm sat} = -1.05$ (see Fig. 15), which is a typical value for ferromagnetic ordering into a domain state, caused by dipolar interactions. Within the scatter of the data, the critical spin polarization was constant below 5 μT, both for magnetic fields parallel and perpendicular to the sample foils. Using the linear, experimentally observed relationship of Eq. (19) between the inverse polarization and temperature, the Curie point $T_{\rm C} = -1.9 \pm 0.4$ nK was obtained.

The magnetic field vs. entropy diagram of silver, for positive and negative spin temperatures, is shown in Fig. 16. The critical entropy is lower for $T > 0$ than for $T < 0$. The difference reflects frustration (Binder and Young, 1986) of antiferromagnetic interactions as well as the influence of dipolar forces which favour ferromagnetism. The critical field B_c of the ferromagnetic phase is determined by the strength of dipolar forces, while B_c of the antiferromagnetic state is caused by the magnitude of the exchange energy. At negative spin temperatures it was

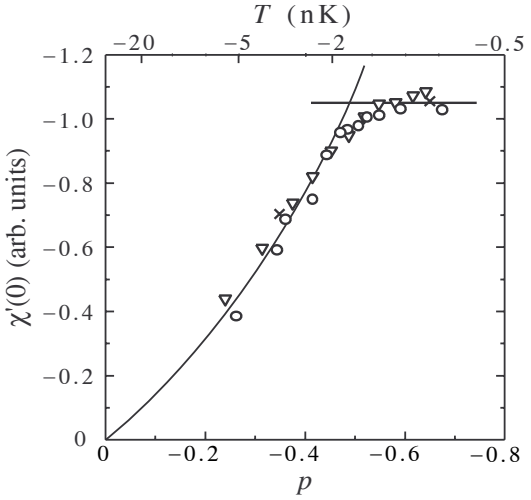

Figure 15. Static susceptibility $\chi'(0)$ of silver vs. polarization p at $T < 0$ (Hakonen et al., 1992). The fitted curve represents the Curie–Weiss law and the straight horizontal line corresponds to the saturation value of susceptibility in the ordered state as predicted by the mean-field theory. An approximate temperature scale is shown at top.

estimated that the critical field $B_c = -\mu_0 M_{\rm sat}/\chi_{\rm sat} = 40\ \mu$T at zero temperature; this value was used when drawing the low entropy end of the transition curve for the ferromagnetic phase. At $T = +0$, $B_c \approx 100\ \mu$T.

The saturation of susceptibility to -1 (see Fig. 15) in the ordered state at $T < 0$ can be explained only by the formation of domains, since otherwise $\chi_{\rm sat}$ would diverge at $T_{\rm C}$ (Viertiö and Oja, 1992). Instead of needles, as at $T > 0$, plate-like domains are expected when energy is maximized at $T < 0$. The size of the domains is large compared to the interatomic spacing but small with respect to the dimensions of the sample. The direction of magnetization $\mathbf{M}$ is degenerate, but the tangential component of $\mathbf{M}$ has to be continuous and the perpendicular component must change sign across a domain wall. Moreover, the total magnetization has to satisfy the condition $\chi_{\rm sat} \approx -1$.

The measured critical entropy, $S_c = 0.82R\ln 2$ at $T < 0$, is higher than the value for the Heisenberg model, $S_c = 0.66R\ln 2$, which indicates that, even though the Ruderman–Kittel exchange is dominating in silver, the dipolar interaction substantially aids in the ordering process at $T < 0$.

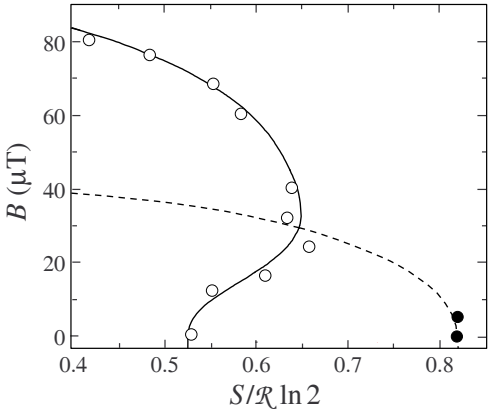

Figure 16. Magnetic field vs. reduced entropy diagram of silver at positive (full curve) and at negative (dashed curve) spin temperatures (Hakonen et al., 1992). At $T > 0$, a long extrapolation to $S = 0$ gives $B_c \approx 100$ μT; the forward "bulge" has not been explained so far.

10 Neutron diffraction on silver

Again, by means of NMR measurements it is not possible to verify the details of the spin structure in silver. Experiments employing scattering of neutrons are necessary, as in copper (see Sect. 8), for this purpose. Tuoriniemi et al. (1995) have recently observed long-range nuclear antiferromagnetic order by neutron diffraction in a single crystal of silver at $T > 0$. For this research the sample again had to be isotopically pure, since ^{107}Ag (51.8%) and ^{109}Ag (48.2%) in natural silver have opposite signs of the spin dependent scattering coefficient b, see Eq. (20), strongly depressing the coherent neutron signal indicating alignment of nuclear spins. 99.7% enriched material of ^{109}Ag was used to grow the $0.7 \times 12 \times 25$ mm^3 single crystal. The $[1, -1, 0]$ axis was parallel to the longest edge of the specimen, which was mounted upright in the cryostat. The plane accessible for neutron diffraction studies was thus spanned by the crystallographic axes $[0, 0, 1]$ and $[1, 1, 0]$.

The experiments were performed at the BER II reactor of the Hahn–Meitner Institut in Berlin (Steiner et al., 1996; Lefmann et al., 1997; Nummila et al., 1997). The setup for these measurements was similar to that used earlier in Risø (see Fig. 8). The diffracted neutrons ($\lambda = 4.4$ Å) were recorded at a fixed scattering angle by a single counter or by a position-sensitive detector. Another counter measured the transmitted neutrons. Experiments could be performed either with unpolarized or

polarized beams.

The sample was cooled in the cascade nuclear demagnetization cryostat illustrated in Fig. 3. New methods of neutron thermometry, based on Eq. (10) which gives the relation between p and T, were developed for these experiments (Lefmann et al., 1997). The neutron beam was the main source of heat, reducing τ_1 to 3 h. Prior to demagnetizations, the diffractometer was aligned to the $(0, 0, 1)$ Bragg position of a Type-I antiferromagnet in an fcc lattice. The build-up of the nuclear polarization could be monitored in situ by measuring transmission of polarized neutrons through the sample (Tuoriniemi et al., 1997).

Figure 17 shows two sets of neutron diffraction data on silver. The nuclei were demagnetized into the ordered state with the final external field $B = 500\ \mu$T along the $[0, 0, 1]$ or $[0, 1, 0]$ directions, and neutron counts were monitored while the spin system warmed up. A clear $(0, 0, 1)$ reflection appeared when demagnetization was

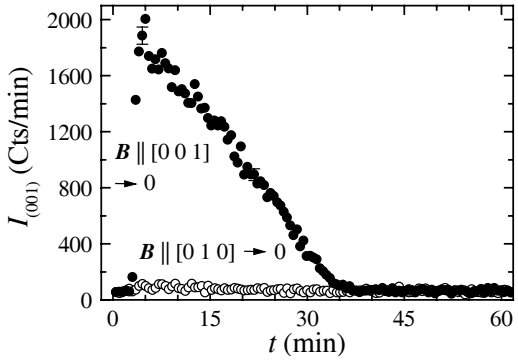

Figure 17. Time dependence of neutron intensity at the $(0, 0, 1)$ Bragg position (Tuoriniemi et al., 1995). The initial polarization $p = 0.91 \pm 0.02$ was first recorded in a 500 μT field in the paramagnetic phase, whereafter $\mathbf{B}$, in the $[0, 0, 1]$ or $[0, 1, 0]$ direction (filled and open circles, respectively), was reduced to zero at $t = 3$ min. The $(0, 0, 1)$ neutron signal appeared immediately below $B_c = 100\ \mu$T, but only when $\mathbf{B} \parallel [0, 0, 1]$ during demagnetization. The silver spins warm up more slowly than the spins of copper (see Fig. 9) because τ_1 is longer in Ag than in Cu.

made with $\mathbf{B}$ parallel to the corresponding ordering vector $\mathbf{k} = (\pi/a)(0, 0, 1)$. The presence of this signal, with mixed Bragg indices, again provided clear proof for Type-I antiferromagnetic order in silver. But the neutron peak was essentially absent when the ordered state was entered from the perpendicular direction $[0, 1, 0]$,

although in zero field the three **k**-vectors, producing the $\{1,0,0\}$ reflections, are equivalent owing to the cubic symmetry. In this respect, the situation in silver was different from that observed in copper. In Ag, no domains of the other two symmetry-equivalent **k** vectors, $(\pi/a)(0,1,0)$ and $(\pi/a)(1,0,0)$, formed during warmup in zero field. It was concluded that the observed antiferromagnetic state had a simple single-**k** structure and that the stable spin configuration was created during demagnetization. The phase transition was apparently of second order.

To demonstrate that the observed intensity indeed was a Bragg peak a position-sensitive detector was used. Time development of the neutron diffraction pattern is shown in Fig. 18. The lineshape of the antiferromagnetic peak is Gaussian, and its width is comparable to that of the $(0,0,2)$ second-order lattice reflection. The critical entropy of ordering was found from the data on transmitted neutrons. Polarization could be deduced from the count rate when the nuclei were aligned

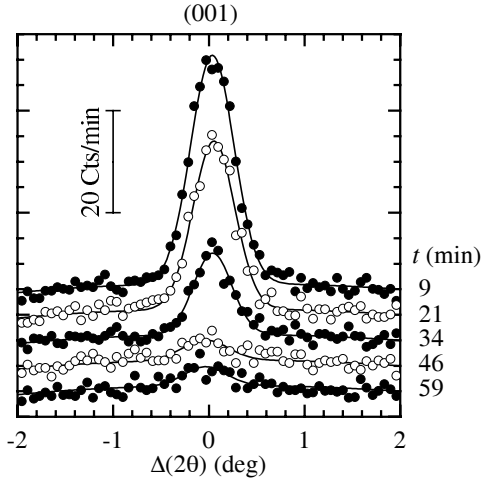

Figure 18. Time evolution (from top to bottom) of the antiferromagnetic Bragg peak of silver in a 30 μT field (Tuoriniemi et al., 1995). The 2θ-dependence of scattered neutrons is plotted as a function of deviation from the $(0,0,1)$ position. The bell-shaped curves are Gaussian fits to counts collected during 6 min intervals; only every second spectrum is shown. For clarity, the successive curves are offset vertically by 5 cts/min. As long as neutrons were observed the spin temperature was below $T_{\rm N} \approx 700$ pK.

by a magnetic field in the paramagnetic state, because the neutron absorption is spin-dependent. For this purpose the 500 μT field was applied at the beginning of each experiment. The orientation of this field also determined the direction along which the ordered state was entered. Polarization was measured again a few times after the disappearance of the antiferromagnetic signal, and the critical value p_c was found by interpolation. The nuclear entropy S could then be calculated from the paramagnetic polarization in 500 μT, see Eq. (11). The field changes were nearly adiabatic ($\Delta S \approx 0.01 R \ln 2$ for each sweep between $B = 0$ and 500 μT), whereby the entropy was known in all fields. In the zero-field experiment of Fig. 18, $p_c = 0.75 \pm 0.02$ was obtained, corresponding to $S_c = (0.54 \pm 0.03) R \ln 2$. The Néel temperature was estimated as $T_{\mathrm{N}} = (700 \pm 80)$ pK. This is higher than 560 pK for natural silver (see Sect. 9) because the strength of the mutual interactions is scaled by the magnetic moment squared, i.e. by a factor of 1.15.

It was interesting to examine the response of the spin system to an applied magnetic field and to its alignment. With $\mathbf{B} \parallel [0,0,1]$, the antiferromagnetic intensity decreased smoothly when approaching the critical field of 100 μT. The spins thus lined up continuously towards the increasing field, as in the spin-flop phase of a weakly anisotropic antiferromagnet. No field-induced phase transitions within the ordered state could be identified. Repetitive field cyclings across the phase boundary to the paramagnetic state did not produce any appreciable hysteresis nor deviations from adiabaticity; therefore, the transition was presumably of second order.

The effect of field orientation was investigated by rotating $\mathbf{B}$ ($B = 50$ μT) with respect to the crystalline axes. In a turn extending from $[-1,-1,0]$ to $[1,1,0]$, the $(0,0,1)$ neutron signal was visible when the magnetic field was aligned between the axes $[-1,-1,1]$ and $[1,1,1]$. Within this arc, the intensity did not vary much. An additional field rotation was made in a perpendicular plane; the neutron signal disappeared about 10° beyond the $[0,-1,1]$ axis. These experiments showed that an antiferromagnetic spin structure with $\mathbf{k} = (\pi/a)(0,0,1)$ was formed when $\mathbf{B}$ was around the $[0,0,1]$ direction within a cone of 110° full opening. Further measurements were made for $B \parallel [0,0,1]$ and for $B \parallel [-0.8,-0.8,1]$; the latter direction is close to the edge of the cone. The allowed field directions thus span a double cone, barely reaching all eight of the $\{1,1,1\}$ directions. Apart from the (0,0,1) reflection, the $(\frac{1}{2},\frac{1}{2},\frac{1}{2})$ Bragg peak of Type-II order and the $(0,\frac{2}{3},\frac{2}{3})$ neutron signal seen in copper were also searched for, but with negative results.

On the basis of these experiments, the magnetic field vs. entropy diagram of silver was constructed. The result is shown in Fig. 19. There is good agreement with earlier susceptibility data (see Sect. 9) on a polycrystalline sample of natural silver. The critical entropy was systematically higher when $\mathbf{B}$ was near the edge of the cone than when the field was parallel to the central axis. The general features

of the NMR experiments on silver were reproduced with the setup at the Hahn–Meitner Institut in the absence of neutrons, but it is somewhat disturbing that the characteristic susceptibility plateau (see Fig. 14) totally disappeared when the neutron beam was on.

The neutron diffraction data on silver can be compared with theoretical work. The observed Type-I ordering vector had been predicted on the basis of measured and calculated interaction parameters (Harmon et al., 1992). The spin structure of the ground-state has been determined by perturbation analysis (Heinilä and Oja, 1993) and by Monte Carlo simulations (Viertiö and Oja, 1992). Both methods indicate that, when $\mathbf{B} \parallel [0,0,1]$, a single-$\mathbf{k}$ configuration is stable in low magnetic fields $B \leq 0.5B_c$. A structure with $\mathbf{k} = (\pi/a)(0,0,1)$ was expected, in perfect agreement with the experimental observations. In higher fields, however, a triple-$\mathbf{k}$ configuration had been predicted. According to the simulations this structure is stable only if $\mathbf{B}$ is within a narrow cone around the $[1,0,0]$-type axes. The measurements, however, did not provide any evidence for the triple-$\mathbf{k}$ state, although it was searched for in field-sweep and field-rotation experiments (Tuoriniemi et al., 1995). In contrast to the complex situation in copper (see Fig. 11), the ordered phase in silver seems to consist of a single Type-I antiferromagnetic structure.

It is not clear which mechanism prevented domains with equivalent $\mathbf{k}$-vectors from forming in $\mathbf{B} = \mathbf{0}$. The fact that the results depended on the direction of the external magnetic field during demagnetization shows that the small dipolar force is strong enough in silver to break isotropy of the RK interaction, see Eqs. (4) and (5), and lock the nuclear spins perpendicular to the corresponding $\mathbf{k}$-vector (Viertiö and Oja, 1992). Perhaps the intermediate $(1, \frac{1}{3}, \frac{1}{3})$-phase in copper (see Fig. 11) effectively "mixed" the spins during demagnetization, allowing different (0,0,1) domains to form.

Neutron diffraction studies of silver at negative spin temperatures have not been attempted so far.

11 Experiments on rhodium

The Helsinki results on rhodium metal, at $T > 0$ and at $T < 0$, are quite interesting as well (Hakonen et al., 1993; Vuorinen et al., 1995). The absolute value of the inverse static susceptibility, as a function of $|T|$, is plotted in Fig. 20. The upper line represents, at $T > 0$, the antiferromagnetic Curie–Weiss law, see Eq. (21), with $\theta = -1.4$ nK. At $T < 0$, the corresponding ferromagnetic dependence is displayed by the dashed line. At low temperatures the Curie–Weiss approximation is known to deviate, especially when $I = 1/2$, from the more accurate results based on high-T series expansions. For negative temperatures, the measured data show

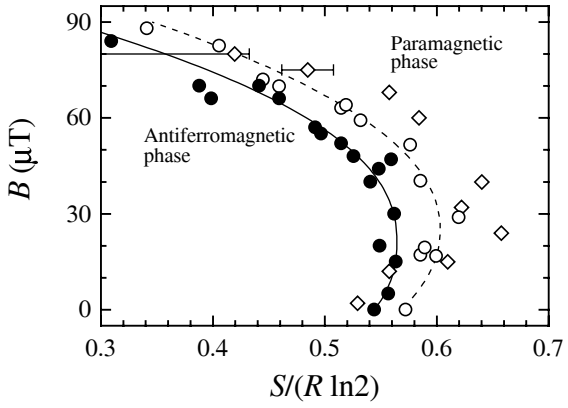

Figure 19. Magnetic field vs. entropy diagram of silver at $T > 0$, based on neutron data (Tuoriniemi et al., 1995). The counts were recorded with $B \parallel [0, 0, 1]$ (•) and $B \parallel [-0.8, -0.8, 1]$ (○). Previous NMR data (Hakonen et al., 1991) are included for comparison (◇). The critical temperature $T_N \approx 700$ pK in zero field.

a crossover from ferro- to antiferromagnetic behaviour at about -5 nK. This indicates that the energy of nuclear spins in rhodium is both minimized and maximized by antiferromagnetic order.

The NMR data on rhodium at $T > 0$ and at $T < 0$ extend to roughly a factor of two closer to the absolute zero than the temperatures reached in the experiments on silver (see Fig. 13). Phase transitions, however, were not seen in rhodium, even though the experimentally achieved polarizations, $p = 0.83$ and $p = -0.60$ at $T > 0$ and at $T < 0$, respectively, were higher than those needed for spontaneous ordering in silver. This is an indication that in Rh the nearest and next-nearest neighbour interactions are of almost equal magnitude but of opposite sign. The transition temperature is thus very low, which explains why no ordering was detected in spite of the record-low, 280 pK, and "record-high", -750 pK, spin temperatures produced in rhodium.

The susceptibility data on Rh can be used to extract the nearest and next-nearest neighbour Heisenberg interaction coefficients J_1 and J_2; the values obtained from experimental results are $J_1/h = -17$ Hz and $J_2/h = 10$ Hz. Molecular-field calculations have been employed to predict the regions of different types of magnetic ordering in the J_2 vs. J_1-plane. This is illustrated in Fig. 21. In an fcc lattice, ferromagnetism is present only when $J_1 > 0$ and $J_2 > -J_1$. The antiferromagnetic part is divided to AF1, AF3, and AF2 regions at $J_2 = 0$ and at $J_2 = J_1/2$, so that

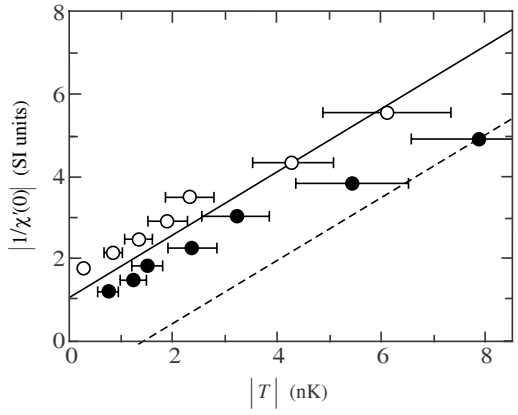

Figure 20. Absolute value of the inverse static susceptibility $|1/\chi'(0)|$ vs. absolute value of temperature for rhodium nuclei, measured at $T > 0$ (○) and at $T < 0$ (●) (Hakonen et al., 1993). The error bars denote the 20% uncertainty in the measurements of temperature.

rhodium lies well inside the AF1 region at $T > 0$. At $T < 0$ the signs of the J's are effectively reversed, and the corresponding point in Fig. 21 is located in the ferromagnetic sector, but rather close to the AF2 antiferromagnetic border.

Spin–lattice relaxation times, measured at positive and negative temperatures, have been investigated in Helsinki on rhodium (Hakonen et al., 1994): Iron impurities shorten substantially τ_1 in small magnetic fields. Previously, this effect has not been studied much in the microkelvin range and below (see, however, Tuoriniemi et al., 1997), in spite of the significance of τ_1 for reaching the lowest nuclear temperatures. A clear difference in τ_1 at $T > 0$ and $T < 0$ was observed.

The spin–lattice relaxation time τ_1 is defined by the relationship

$$d(1/T)/dt = -(1/\tau_1)(1/T - 1/T_e). \tag{22}$$

Since $T_e \gg T$ and $p \propto 1/T$, one finds the exponential time dependence $d\ln p/dt = -(1/\tau_1)$, i.e., $p \propto \exp(-t/\tau_1)$. Experimental data are shown in Fig. 22. The spin–lattice relaxation time was found by fitting a straight line to about 10 successive data points on the $\log p$ vs. t plot. The results show clearly that τ_1 is longer at $T < 0$ than at $T > 0$ and that the spin–lattice relaxation slows down with decreasing polarization when $T > 0$. The most striking result of these relaxation time measurements is that τ_1 is longer when $T < 0$. This finding is difficult to explain since all theories predict equal behaviour on both sides of the absolute zero.

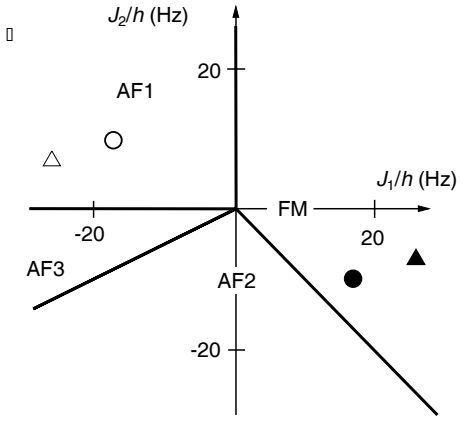

Figure 21. Molecular field calculations for Ag and Rh spins (Vuorinen et al., 1995). Antiferromagnetic regions are denoted by AF1, AF2, and AF3, respectively, whereas FM refers to ferromagnetic ordering. Interaction parameters for rhodium (○) and silver (△) spins are plotted in the figure; open and filled symbols refer to positive and negative temperatures, respectively.

The next step is reaching the ordering transitions at $T > 0$ and at $T < 0$ in rhodium. This should not be too difficult a task with the new YKI cryostat.

12 Concluding remarks

The weakest interactions in solids, by far, are between nuclear spins. Consequently, the time scales for the onset of order or changes therein are long, compared to electronic magnets. Many new phenomena thus become experimentally accessible in studies of nuclear magnets. Determination of the ordered ground state requires special low temperature techniques, extending to nano- and even picokelvin temperatures. The magnetic susceptibility and neutron diffraction and transmission experiments on copper and silver, and NMR measurements on rhodium, have revealed the intricacies of spontaneous magnetic ordering phenomena in these simple metals. It has become obvious that nuclear magnets are not just another class of magnetic materials, but represent systems whose properties add new insights to our knowledge of magnetic ordering and the kinetics of phase transitions.

In copper the phase diagram is surprisingly complex (see Fig. 7); hysteresis and time dependent phenomena have been detected. The close competition between the antiferromagnetic exchange interaction and the ferromagnetic dipolar force is

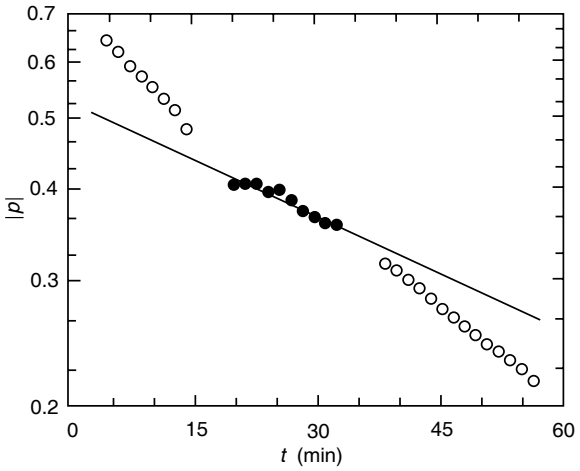

Figure 22. Polarization $|p|$ of rhodium spins as a function of time measured in a magnetic field of 40 μT at $T > 0$ (○) and at $T < 0$ (●) (Hakonen et al., 1994). The straight line is a least-squares fit to the data at $T < 0$.

probably responsible for the complex behaviour of copper. In silver the phase diagram is simpler (see Fig. 16), remarkably stable, but with an unexpected "bulge" at $T > 0$. Successful magnetic susceptibility measurements at negative spin temperatures in silver and rhodium have clarified thermodynamics at $T < 0$.

Research on nuclear magnetism in metals at nano- and picokelvin temperatures continues. With copper there is the mystery (see Sect. 8) of the missing $(1, 0, 0)$ Bragg reflection along the $\{1, 1, 1\}$ field directions. The neutron diffraction work on silver, described in Sect. 10, is not completed; experiments at the Hahn–Meitner Institut continue. More measurements are due in the high symmetry directions $\{1, 1, 0\}$ and $\{1, 1, 1\}$ over the whole range of fields. The stability of magnetic domains in zero field will be investigated as well. Experiments using polarized neutrons, with a full polarization analysis, will be made to determine the directions of the ordered nuclear spins in relation to the crystallographic axes. An ambitious project, also involving polarized neutrons, is to investigate the ferromagnetic structure of silver at negative spin temperatures.

The next goal for the susceptibility measurements in Helsinki is to observe nuclear spin ordering in rhodium. Another experiment which is on the agenda is susceptibility measurements on gold. Here one has the additional bonus that superconductivity might be observed. According to earlier experiments (Buchal et

al., 1982) on alloys rich in noble metals, the superconducting transition temperature for pure gold should be about five orders of magnitude higher than for silver or copper. The problem is to obtain a sufficiently pure specimen so that electronic magnetic impurities would not destroy superconductivity.

Another very promising system is platinum. In this metal there is only one magnetic isotope, ^{195}Pt; the other stable isotopes are nonmagnetic. This means that it is possible to prepare platinum specimens in which the magnetic component varies between zero and 100%. In copper and silver, one cannot change the magnetic concentration because in these metals all stable isotopes have non-integral nuclear spins and, besides, the magnetic moments of the two stable isotopes in both metals are within 7% and 13% of each other, respectively.

In platinum a study of ordering as a function of the magnetic constituent is interesting because the system would provide a very pure model of a spin glass. Unfortunately, however, the properties of platinum are strongly influenced by small concentrations of electronic magnetic impurities. In addition, because of the small value of Korringa's constant, see Eq. (2), $\kappa = 0.03$ sK in Pt, nuclear spins and conduction electrons reach thermal equilibrium quickly, so one might need a three-stage nuclear refrigerator for these experiments.

There are other possibilities as well. For example, the interplay between superconductivity and magnetism could be investigated: By reversing the sign of temperature, the nuclear spin order might be changed from antiferro- to ferromagnetism or vice versa, and the effect of this transformation on the superconducting properties could be investigated. Unfortunately, owing to supercooling, measurements of this type did not succeed in rhodium, even though the conduction electron and lattice temperature in the Helsinki experiments was considerably lower than 325 μK, the critical temperature for superconductivity in rhodium. In $AuIn_2$, superconductivity did not affect nuclear ordering (Herrmannsdörfer et al., 1995). There are several other simple metals for which one can expect important progress in studies of nuclear ordering; these include thallium, scandium, and yttrium. The new YKI cryostat, which has just started operating in Helsinki, and the improvements made in the neutron diffraction setup at the Hahn–Meitner Institut in Berlin will open new possibilities for still more ambitious experiments.

It has been argued, sometimes, that negative temperatures are fictitious quantities because they do not represent true thermal equilibrium in a sample consisting of nuclei, conduction electrons, and the lattice. However, the experiments on silver, in particular, show conclusively that this is not the case. The same interactions produce ferro- or antiferromagnetic order, depending on whether the spin temperature is negative or positive. In fact, the realm of negative spin temperatures offers interesting new possibilities for studies of magnetism in metals.

Acknowledgements

I wish to thank Pertti Hakonen, Kaj Nummila, and Aarne Oja for useful comments and Juha Martikainen for improving some of the figures. My one-year stay at the Hahn–Meitner Institut in Berlin, during which time I wrote most of this review, was made possible by a generous Research Award from the Alexander von Humboldt Stiftung.

References

Abragam A, 1987: Proc. Roy. Soc. London **412**, 255
Andres K, and Bucher E, 1968: Phys. Rev. Lett. **21**, 1221
Andres K and Lounasmaa OV, 1982: Prog. Low. Temp. Phys. **8**, 221
Annila AJ, Clausen KN, Lindgård PA, Lounasmaa OV, Oja AS, Siemensmeyer K, Steiner M, Tuoriniemi JT and Weinfurter H, 1990: Phys. Rev. Lett. **64**, 1421
Annila AJ, Clausen KN, Oja AS, Tuoriniemi JT and Weinfurter H, 1992: Phys. Rev. B **45**, 7772
Binder K and Young AP, 1986: Rev. Mod. Phys. **58**, 801
Bloembergen N and Rowland TJ, 1955: Phys. Rev. **97**, 1679
Bouffard V, Fermon C, Gregg JF, Jacquinot JF and Roinel Y, 1994: *NMR and More in Honour of Anatole Abragam*, eds. M. Goldman and M. Porneuf (Les Editions de Physique, France) p. 81
Buchal Ch, Mueller RM, Pobell F, Kubota M and Folle HR, 1982: Solid State Commun. **42**, 43
Ehnholm GJ, Ekström JP, Jacquinot JF, Loponen MT, Lounasmaa OV and Soini JK, 1979: Phys. Rev. Lett. **42**, 1702
Ehnholm GJ, Ekström JP, Jacquinot JF, Loponen MT, Lounasmaa OV and Soini JK, 1980: J. Low Temp. Phys. **39**, 417
Frisken SJ and Miller DJ, 1986: Phys. Rev. Lett. **57**, 2971
Frisken SJ and Miller DJ, 1988: Phys. Rev. Lett. **61**, 1017
Goldman M, 1970: *Spin Temperature and Nuclear Magnetic Resonance in Solids* (Clarendon Press, Oxford)
Hakonen PJ and Lounasmaa OV, 1994: Science **265**, 1821
Hakonen PJ, Lounasmaa OV and Oja AS, 1991: J. Magn. Magn. Mater. **100**, 394
Hakonen PJ, Nummila KK, Vuorinen RT and Lounasmaa OV, 1992: Phys. Rev. Lett. **68**, 365
Hakonen PJ, Vuorinen RT and Martikainen JE, 1993: Phys. Rev. Lett. **70**, 2818
Hakonen PJ, Vuorinen RT and Martikainen JE, 1994: Europhys. Lett. **25**, 551
Hakonen PJ, Yin S and Lounasmaa OV, 1990: Phys. Rev. Lett. **64**, 2707
Hakonen PJ, Yin S and Nummila KK, 1991: Europhys. Lett. **15**, 677
Harmon BN, Wang XW and Lindgård PA, 1992: J. Magn. Magn. Mater. **104-107**, 2113
Heinilä MT and Oja AS, 1993: Phys. Rev. B **48**, 7227
Heinilä MT and Oja AS, 1996: Phys. Rev. B **54**, 1
Herrmannsdörfer TP, Smeibidl P, Schröder-Smeibidl B and Pobell F, 1995: Phys. Rev. Lett. **74**, 1665
Huiku MT, Jyrkkiö TA, Kyynäränen JM, Loponen MT, Lounasmaa OV and Oja AS, 1986: J. Low Temp. Phys. **62**, 433
Huiku MT, Jyrkkiö TA, Kyynäräinen JM, Oja AS and Lounasmaa OV, 1984: Phys. Rev. Lett. **53**, 1692
Huiku MT and Loponen MT, 1982: Phys. Rev. Lett. **49**, 1288

Jyrkkiö TA, Huiku MT, Lounasmaa OV, Siemensmeyer K, Kakurai K, Steiner M, Clausen KN and Kjems JK, 1988: Phys. Rev. Lett. **60**, 2418
Jyrkkiö TA, Huiku MT, Siemensmeyer K and Clausen KN, 1989: J. Low Temp. Phys. **74**, 435
Kjäldman LH and Kurkijärvi J, 1979: Phys. Lett. **71A**, 454
Koike Y, Suzuki H, Abe S, Karaki Y, Kubota M and Ishimoto H, 1995: J. Low Temp. Phys. **101**, 617
Kurti N, Robinson FN, Simon FE and Spohr DA, 1956: Nature **178**, 450
Lefmann K, Tuoriniemi JT, Nummila KK and Metz A, 1997: Z. Phys. (in press)
Lindgård PA, 1988: Phys. Rev. Lett. **61**, 629
Lindgård PA, 1992: J. Magn. Magn. Mater. **104-107**, 2109
Lindgård PA, Wang XW and Harmon BN, 1986: J. Magn. Magn. Mater. **54-57**, 1052
Lounasmaa OV, 1974: *Experimental Principles and Methods Below 1 K* (Academic Press, London)
Lounasmaa OV, 1989: Physics Today **42**, 26
Lounasmaa OV, Hakonen P, Nummila K, Vuorinen R and Martikainen J, 1994: Physica B **194-196**, 291
Nummila KK, Tuoriniemi JT, Vuorinen RT, Lefmann K, Metz A and Rasmussen FB, 1997: (to be published).
Oja AS, Annila AJ and Takano Y, 1990: Phys. Rev. Lett. **65**, 1921
Oja AS and Lounasmaa OV, 1997: Rev. Mod. Phys. **69**
Oja AS and Viertiö HE, 1993: Phys. Rev. B **47**, 237
Price DL and Sköld K, 1986: in *Neutron Scattering: Methods of Experimental Physics*, eds. K. Sköld and D.L. Price (Academic Press, London) Vol. 23, Part A, p. 1
Purcell EM and Pound RV, 1951: Phys. Rev. **81**, 279
Ramsey NF, 1956: Phys. Rev. **103**, 20
Schröder-Smeibidl B, Smeibidl P, Eska G and Pobell F, 1991: J. Low Temp. Phys. **85**, 311
Slichter, C.P., 1990: *Principles of Magnetic Resonance* (Springer Verlag, Berlin) p. 219
Steiner M, 1990: Physica Scripta **42**, 367
Steiner M, 1993: Int. J. Mod. Phys. B **7**, 2909
Steiner M, Metz A, Siemensmeyer K, Lounasmaa OV, Tuoriniemi JT, Nummila KK, Vuorinen RT, Clausen KN, Lefmann K and Rasmussen FB, 1996: J. Appl. Phys. **79**, 5078
Tuoriniemi JT, Nummila KK, Lefmann K, Vuorinen RT, and Metz A, 1997: Z. Phys. (in press)
Tuoriniemi JT, Nummila KK, Vuorinen RT, Lounasmaa OV, Metz A, Siemensmeyer K, Steiner M, Lefmann K, Clausen KN and Rasmussen FB, 1995: Phys. Rev. Lett. **75**, 3744
Van der Zon CM, Van Velzen GD and Wenckebach WTh, 1990: J. Phys. (Paris) **51**, 1479
Van Vleck JH, 1957: Nuovo Cimento Suppl. **6**, 1081
Viertiö HE and Oja AS, 1987: Phys. Rev. B **36**, 3805
Viertiö HE and Oja AS, 1990: Phys. Rev. B **42**, 6857
Viertiö HE and Oja AS, 1992: J. Magn. Magn. Mater. **104-107**, 915
Viertiö HE and Oja AS, 1993: Phys. Rev. B **48**, 1062
Vuorinen RT, Hakonen PJ, Yao W and Lounasmaa OV, 1995: J. Low Temp. Phys. **98**, 449
Windsor CG, 1986: in *Neutron Scattering: Methods of Experimental Physics*, eds. K. Sköld and D.L. Price (Academic Press, London) Vol. 23, Part A, p. 197